UNIVERSITÀ DEGLI STUDI DI NAPOLI FEDERICO II
DIPARTIMENTO DI INGEGNERIA ELETTRICA E TECNOLOGIE DELL'INFORMAZIONE
SCUOLA POLITECNICA E DELLE SCIENZE DI BASE

Technical paper for
Dinamica e Controllo Non Lineare

Analysis and control of a biodynamical model of HIV-1

Candidato:
Michele Marolla

Anno Accademico 2020–2021

Contents

List of Figures

Chapter 1

Introduction

Over the last years, significant advances has been made in our understanding of human immunodeficiency virus (HIV-1) infection. The research led to new therapies, including highly active antiretroviral therapy (HAART) drug therapy. It is well known that HIV-1 cell production in an infected individual is the result of a dynamic process: the effort in modeling the interaction between HIV-1 and some specific cells is fundamental in developing new and better treatments.

Developing a model able to describe the HIV-1 infection evolution is crucial to determine the state of health of an individual, verify the effects of different therapeutic drug regimes, and predict the evolution of the infection.

In this paper, the prey-predator like model proposed by de Souza [5] is considered.

In Chapter 1, the system's model is derived, and its main properties discussed.

In Chapter 2, an open-loop system analysis is performed. In particular, system's equilibria and their stability are analyzed, and a phase portrait is depicted. Also, a bifurcation analysis is carried out.

In Chapter 3, the control problem is tackled. The performances of a linear controller designed on the linearized system is compared to nonlinear controllers: in particular, a feedback linearization scheme and its adaptive extension are considered.

Finally, Chapter 4 draws conclusions about the controllers comparison, and some possible further developments are proposed.

1.1 Model derivation

It is known that HIV-1 replicates itself destroying a large number of the CD4 lymphocyte cells; on the other hand, this replication is counteracted by a natural defensive response, attributed to the CD8 lymphocyte cells.

Parameters	Value	Unit	Description
a	0.25	year^{-1}	death rate of CD4 cells
b	50	$\text{ml}/10^7$ copies·year	rate of CD4 cells infection
c	0.25	year^{-1}	death rate of CD8 cells
d	10	$\text{ml}/10^7$ copies·year	rate of CD8 increase in response to viral load
e	0.01	mm^3/ cells·year	rate of increase of viral load
f	0.0045	mm^3/ cells·year	rate of decrease of viral load
x_{10}	1000	cells/mm^3	CD4 equilibrium value
x_{20}	550	cells/mm^3	CD8 equilibrium value

Table 1.1: Description of variables and parameters.

Let's denote by x_1, x_2 and x_3 the CD4 population, CD8 population, and HIV-1 viral load, respectively. In absence of HIV-1 infection (i.e., $x_3 = 0$), the lymphocytes are regulated to their normal levels x_{10} and x_{20}. The dynamics of this regulation has a time constant equal to $1/a$ for CD4 and $1/c$ for CD8 lymphocytes.

In case of infection, the encounters between CD4 and HIV-1 cells affect negatively the growth rate of CD4; the probability that this encounters occur is proportional by a factor b to the product of the populations of HIV-1 and CD4.

Similarly, an encounter between CD8 and HIV-1 will trigger an increase in production of CD8 cells, and a destruction of HIV-1 cells. Again, the probability that this encounters occur is proportional by a factor d to the product of the populations of HIV-1 and CD8.

In the end, HIV-1 "feeds on" CD4 cells and is destroyed by CD8 cells; the parameters relating the growth rate of HIV-1 population with CD4 and CD8 are e and f respectively.

Collecting all these information, the interaction between HIV-1, CD4 and CD8 cells can be modeled as a prey-predator like model as:

$$\begin{cases} \dot{x}_1 = a(x_{10} - x_1) - bx_1x_3 \\ \dot{x}_2 = c(x_{20} - x_2) + dx_2x_3 \\ \dot{x}_3 = x_3(ex_1 - fx_2) \end{cases} \tag{1.1}$$

The meaning of each variable and parameter used in the system is explained in Table (1.1), along with their numerical values as proposed in [5].

Notice that, while CD4 and CD8 cell counts are represented in cells/mm^3, the viral load may be represented for an easier visual comparison in copies/ml (i.e., 10^7 cells/mm^3).

1.1.1 Model properties

Of course, all the x_i variables, with $i = 1, 2, 3$ are non-negative quantities, and all the parameters are positive. Moreover:

Theorem 1. *The set $x > 0$ is a positive invariant set for the system (1.1).*

Proof. If $x_i = 0$ it is $\dot{x}_i > 0, \forall i$; this means that the vector field always points inside the positive octant, and thus the non-negative property for the system's state is always satisfied. □

Also, it can be proved that:

Theorem 2. *The trajectories of the system (1.1) are such that:*

$$\left.\begin{array}{l} x_1(0) < x_{10} \Longrightarrow x_1(t) < x_{10} \\ x_2(0) > x_{20} \Longrightarrow x_2(t) > x_{20} \end{array}\right\} \forall t > 0 \tag{1.2}$$

Proof. Since it $x_1 > 0, x_3 > 0$, and the parameters a and b are positive constants, it is $\dot{x}_1(t) < 0$ whenever $x_1(t)$ approaches x_{10}. In a similar way, because $x_2 > 0, x_3 > 0$ and also $c, d > 0$, then $\dot{x}_2(t) > 0$ whenever $x_2(t)$ approaches x_{20}. □

From these two theorems, one can conclude that the set:

$$\{0 \leq x_1 \leq x_{10},\, x_2 \geq x_{20},\, x_3 \geq 0\} \tag{1.3}$$

is a positive invariant set for system (1.1)

This observation can be used in the system's analysis and control, and it is validated also from practical experience: in fact, in a HIV-1 infected patient the CD4 count is much less than the healthy value, while instead the CD8 count is much more than the healthy value.

Actually, it is possible to find a smaller invariant set for the system.

Theorem 3. *The set*

$$\{0 \leq x_1 \leq x_{10},\, x_{20} \leq x_2 \leq \frac{\lambda}{\psi},\, 0 \leq x_3 \leq \frac{\lambda}{\psi}\}$$

is a positive invariant set for the system (1.1), where:

$$\lambda = a x_{10} + c x_{20} \qquad \psi = \min\{a, c, (b-e)x_{10} - (d-f)x_{20}\}$$

Proof. Denote by P the total cell population: $P = x_1 + x_2 + x_3$. Differentiating with respect to time yields:

$$\dot{P} = \dot{x}_1 + \dot{x}_2 + \dot{x}_3 = ax_{10} + cx_{20} - ax_1 - cx_2 - [(b-e)x_1 + (f-d)x_2]x_3 \quad (1.4)$$

For Theorem (2), it is $x_1 \leq x_{10}$ and $x_2 \geq x_{20}$; also, it is $b > e$ and $d > f$. For these reasons, one can write:

$$\begin{aligned} \dot{P} &\leq (ax_{10} + cx_{20}) - ax_1 - cx_2 - [(b-e)x_{10} + (f-d)x_{20}]x_3 \\ &\leq \lambda - \psi P \end{aligned} \quad (1.5)$$

where:

$$\lambda = ax_{10} + cx_{20} \qquad \psi = \min\{a, c, (b-e)x_{10} - (d-f)x_{20}\} > 0 \quad (1.6)$$

Applying the Comparison lemma [3, p. 102], an upper bound for the cell population can be found:

$$\dot{P} \leq \lambda - \psi P \quad \Longrightarrow \quad P(t) \leq \frac{\lambda}{\psi} \quad \forall t \quad (1.7)$$

For this reason, we can conclude that the set

$$\{0 \leq x_1 \leq x_{10},\, x_{20} \leq x_2 \leq \frac{\lambda}{\psi},\, 0 \leq x_3 \leq \frac{\lambda}{\psi}\}$$

is positive invariant for the system.

□

1.1.2 Coordinate transformation

For analysis and control purposes, it can be useful to rewrite the system in such a way that the virus-free equilibrium $x_H^* = (x_{10}, x_{20}, 0)^T$ (see Section 2.1) coincides with the origin of the state space.

For this reason, consider a new state vector defined as:

$$z = \begin{bmatrix} z_1 \\ z_2 \\ z_3 \end{bmatrix} = \begin{bmatrix} x_1 - x_{10} \\ x_2 - x_{20} \\ x_3 \end{bmatrix} \quad (1.8)$$

Rewriting the system's equations (1.1) with the new coordinates yields:

$$\begin{cases} \dot{z}_1 &= -az_1 - b(z_1 + x_{10})z_3 \\ \dot{z}_2 &= -cz_2 + d(z_2 + x_{20})z_3 \\ \dot{z}_3 &= z_3[e(z_1 + x_{10}) - f(z_2 + x_{20})] \end{cases} \quad (1.9)$$

The virus-free equilibrium corresponds now to $z_H^* = (0, 0, 0)^T$. The aim of the control is to force z to converge to zero, that is, to force x to converge to $x_H^* = (x_{10}, x_{20}, 0)^T$.

Chapter 2

Open-loop analysis

In this chapter, an open-loop analysis of the system is carried out. In particular, the system's equilibria will be found, and their stability properties discussed; numerical simulations will be used in order to obtain a phase portrait representation of the system. Also, internal stability and bifurcations will be investigated.

2.1 Equilibria and stability

Equilibria can be found solving the system of equations $\dot{x} = 0$. In particular, considering the third equation:

$$\dot{x}_3 = x_3(ex_1 - fx_2) = 0$$

it is clear that the system has two equilibrium points.

Virus-free equilibrium

The first equilibrium corresponds to $x_3 = 0$ and thus represents a virus-free, healty condition:

$$x_H^* = \begin{pmatrix} x_{10} & x_{20} & 0 \end{pmatrix}^T \tag{2.1}$$

The Jacobian of the system is :

$$J(x) = \begin{bmatrix} -a - bx_3 & 0 & -bx_1 \\ 0 & -c + dx_3 & dx_2 \\ ex_3 & -fx_3 & ex_1 - fx_2 \end{bmatrix} \tag{2.2}$$

In particular, the Jacobian evaluated in the virus-free equilibrium is:

$$J(x_H^*) = \begin{bmatrix} -a & 0 & -bx_{10} \\ 0 & -c & dx_{20} \\ 0 & 0 & ex_{10} - fx_{20} \end{bmatrix} \tag{2.3}$$

Since this is a triangular matrix, its eigenvalues are:

$$\lambda_1 = -a, \quad \lambda_2 = -c, \quad \lambda_3 = ex_{10} - fx_{20} \tag{2.4}$$

Because λ_1 and λ_2 are both negative, the stability of this equilibrium depends on the sign of λ_3.

In particular, if $\alpha = ex_{10} - fx_{20} < 0$, the point is a stable node: this means that, in case of infection, the organism's immunitary response is able to annihilate the virus. Unfortunately, this is not the typical case: in the vast majority of realistic scenarios, in fact, it is $\alpha > 0$, and thus the equilibrium is unstable.

Considering the numerical value defined in Table (1.1) for the parameters, the Jacobian eigenvalues and eigenvectors are the following:

$$\lambda_1 = -a = -0.25 \qquad \Rightarrow v_1 = \begin{pmatrix} 1 & 0 & 0 \end{pmatrix}^T \tag{2.5}$$

$$\lambda_2 = -c = -0.25 \qquad \Rightarrow v_2 = \begin{pmatrix} 0 & 1 & 0 \end{pmatrix}^T \tag{2.6}$$

$$\lambda_3 = ex_{10} - fx_{20} = 7.525 \qquad \Rightarrow v_3 = \begin{pmatrix} -0.994 & 0.1093 & 0.0002 \end{pmatrix}^T \tag{2.7}$$

Since we have two negative eigenvalues and one positive eigenvalue, the equilibrium can be classified as a saddle point.

While the CD4 and CD8 cell population would tend to their normal value, even a small value of viral load make the system's trajectories diverge from the virus-free equilibrium, dragged by the unstable manifold along the v_3 direction, characterized by an increase of CD8 and HIV-1 count and a decrease of CD4 count. In other words, the plane $x_3 = 0$ is the stable manifold of this saddle equilibrium.

Infected equilibrium

The second equilibrium can be derived by solving the system of equations $\dot{x} = 0$ while imposing $x_3 > 0$, and thus corresponds to an infected condition.

In this case, x_1 and x_2 equilibrium values can be found as functions of the viral load; the equilibrium point is $x_I^* = (x_1^*, x_2^*, x_3^*)^T$, where:

$$x_1^* = \frac{ax_{10}}{a + bx_3^*}, \qquad x_2^* = \frac{cx_{20}}{c - dx_3^*} \tag{2.8}$$

Imposing $\dot{x}_3 = 0 \Rightarrow ex_1^* - fx_2^* = 0$, one can rewrite the equilibrium in terms of the system's parameters, getting the following expressions:

$$x_1^* = \frac{adex_{10} + bcfx_{20}}{e(ad + bc)}, \quad x_2^* = \frac{adex_{10} + bcfx_{20}}{f(ad + bc)}, \quad x_3^* = \frac{ac(ex_{10} - fx_{20})}{adex_{10} + bcfx_{20}} \tag{2.9}$$

As said before, in order for the equilibrium viral load to be positive, it is necessary that $ex_{10} - fx_{20} > 0$; otherwise, the virus-free condition would be the only existing equilibrium. A more in-depth analysis about this aspect is carried out in Section 2.4.

Considering the numerical values defined in Table (1.1), the Jacobian eigenvalues are the followings:

$$\lambda_1 = -0.2906 + 1.3266i \tag{2.10}$$
$$\lambda_2 = -0.2906 - 1.3266i \tag{2.11}$$
$$\lambda_3 = -0.2550 \tag{2.12}$$

This equilibrium has two complex conjugate eigenvalues λ_1, λ_2 with negative real part, and one real negative eigenvalue λ_3.

This means that the infected equilibrium is stable: it attracts the nearby trajectories with an exponential convergence along the direction v_3 (i.e., the eigenvector associated with λ_3), and stable focus-like dynamics along the other two directions.

This behaviour can be clearly seen in the figures in Section 2.3.

2.2 Internal stability

In this section, internal stability or *Lyapunov* stability of the system is investigated. In particular, we are interested in estimating the range of asymptotic stability of the system's equilibria.

2.2.1 Virus-free equilibrium

Theorem 4. *If $ex_{10} - fx_{20} < 0$, then the only-existing virus-free equilibrium $[x_{10}, x_{20}, 0]^T$ for system (1.1) is globally asymptotically stable.*

Proof. Consider the following Lyapunov candidate function:

$$V = p_1\Big(x_1 - x_{10} - x_{10}\log\frac{x_1}{x_{10}}\Big) + p_2\Big(x_2 - x_{20} - x_{20}\log\frac{x_2}{x_{20}}\Big) + p_3x_3 \tag{2.13}$$

where $p_i > 0$, $i = 1, 2, 3$ are positive scalars to be determined; for lymphocytes population, logarithmic terms has been chosen, as proposed in [2] for many-species systems.

Since it is:

$$x - k - k\log\frac{x}{k} = 0 \qquad x = k \tag{2.14}$$
$$x - k - k\log\frac{x}{k} > 0 \qquad \forall x > 0,\, k > 0 \tag{2.15}$$

then, for the system's non-negative property:

$$\begin{aligned} V &= 0 && x = [x_{10}, x_{20}, 0]^T \\ V &> 0 && \forall x \neq [x_{10}, x_{20}, 0]^T \end{aligned}$$

Differentiating the expression of V with respect to time, and collecting similar terms yields:

$$\begin{aligned} \dot{V} = p_1 \frac{x_1 - x_{10}}{x_1} \dot{x}_1 + p_2 \frac{x_2 - x_{20}}{x_2} \dot{x}_2 + p_3 \dot{x}_3 = \\ = -p_1 a \frac{(x_{10} - x_1)^2}{x_1} - p_2 c \frac{(x_{20} - x_2)^2}{x_2} + (p_1 b x_{10} - p_2 d x_{20}) x_3 \\ + (p_3 e - p_1 b) x_1 x_3 + (p_2 d - p_3 f) x_2 x_3 \end{aligned} \quad (2.16)$$

Choosing $p_1 = (e/b)p_3$, $p_2 = (f/d)p_3$, and $p_3 = 1$ for simplicity, we get rid of the mixed terms in $x_1 x_3$ and $x_2 x_3$; the previous expression is reduced to:

$$\dot{V} = -\frac{ae}{b} \frac{(x_{10} - x_1)^2}{x_1} - \frac{cf}{d} \frac{(x_{20} - x_2)^2}{x_2} + (e x_{10} + f x_{20}) x_3 \quad (2.17)$$

Since we have assumed $e x_{10} + f x_{20} < 0$, then the Lyapunov function V is negative definite. Also, since it is:

$$\lim_{x \to \infty} \Big(x - k - k \log \frac{x}{k} \Big) = \infty$$

the Lyapunov function V is radially unbounded, and so the virus-free equilibrium is globally asymptotically stable. □

2.2.2 Infected equilibrium

Theorem 5. *If $e x_{10} - f x_{20} > 0$, the infected equilibrium $[x_1^*, x_2^*, x_3^*]^T$ for system (1.1) is asymptotically stable $\forall x_3 > 0$.*

Proof. Consider the following Lyapunov candidate function:

$$V = \sum_i p_i \Big(x_i - x_i^* - x_i^* \log \frac{x_i}{x_i^*} \Big) \quad (2.18)$$

where $p_i > 0$, $i = 1, 2, 3$.

Differentiating the expression of V with respect to time:

$$\dot{V} = p_1 \frac{x_1 - x_1^*}{x_1}\dot{x}_1 + p_2 \frac{x_2 - x_2^*}{x_2}\dot{x}_2 + p_3 \frac{x_3 - x_3^*}{x_1}\dot{x}_3 =$$
$$= -p_1 a \frac{(x_1 - x_1^*)(x_1 - x_{10})}{x_1} - p_3 e x_3^* x_1 - p_2 c \frac{(x_2 - x_2^*)(x_2 - x_{20})}{x_2} + p_3 f x_3^* x_2$$
$$+ (p_1 b x_1^* - p_2 d x_2^*) x_3 + (p_3 e - p_1 b) x_1 x_3 + (p_2 d - p_3 f) x_2 x_3 \quad (2.19)$$

Choosing $p_1 = (e/b)p_3$, $p_2 = (f/d)p_3$, and $p_3 = 1$, we get rid of the mixed terms. Also, recalling the expression of x_1^* and x_2^*, it is:

$$p_1 b x_1^* - p_2 d x_2^* = e x_1^* - f x_2^* = 0$$

Thus we get:

$$\dot{V} = \dot{V}_1(x_1) + \dot{V}_2(x_2) \quad (2.20)$$

where:

$$\dot{V}_1(x_1) = -\frac{ae}{b}\frac{(x_1 - x_1^*)(x_1 - x_{10})}{x_1} - e x_3^* x_1 \quad (2.21)$$
$$\dot{V}_2(x_2) = -\frac{cf}{d}\frac{(x_2 - x_2^*)(x_2 - x_{20})}{x_2} + f x_3^* x_2 \quad (2.22)$$

Consider now the function $\dot{V}_1(x_1)$: this is a function of the sole variable x_1, and it can be rewritten as:

$$\dot{V}_1 = -\frac{ae}{b}\Big(\frac{x_{10}}{x_1^*}x_1 - (x_{10} + x_1^*) + \frac{x_{10}x_1^*}{x_1}\Big) \quad (2.23)$$

We want to find an upper bound for $\dot{V}_1$. Differentiating with respect to x_1, and imposing this derivative to be equal to zero yields:

$$\frac{\partial \dot{V}_1}{\partial x_1} = -\frac{ae}{b}\Big(\frac{x_{10}}{x_1^*} - \frac{x_{10}x_1^*}{x_1^2}\Big) = -\frac{ae}{b}\frac{x_{10}}{x_1^*}\frac{(x_1 + x_1^*)(x_1 - x_1^*)}{x_1^2} = 0 \quad (2.24)$$

Thus, the point $x_1 = x_1^*$ is a maximum for $\dot{V}_1$. Substituting its expression:

$$\dot{V}_1 \leq -\frac{ae}{b}(x_{10} - x_1^*) < 0 \quad (2.25)$$

The same reasoning can be applied to the function $\dot{V}_2(x_2)$. It can be rewritten as:

$$\dot{V}_2 = -\frac{cf}{d}\Big(\frac{x_{20}}{x_2^*}x_2 - (x_{20} + x_2^*) + \frac{x_{20}x_2^*}{x_2}\Big) \quad (2.26)$$

Differentiating with respect to x_2 and imposing this derivative to be equal to zero, the maximum for $\dot{V}_2$ is given by $x_2 = x_2^*$, and thus:

$$\dot{V}_2 \leq -\frac{cf}{d}(x_{20} - x_2^*) \tag{2.27}$$

Combining Equations (2.25) and (2.25), and substituting the expression of x_1^* and x_2^* as in Equation (2.9):

$$\begin{aligned}\dot{V} = \dot{V}_1 + \dot{V}_2 \leq -\frac{ae}{b}(x_{10} - x_1^*) - \frac{cf}{d}(x_{20} - x_2^*) = \\ = -\frac{ae}{b}\frac{bc}{(ad+bc)e}(ex_{10} - fx_{20}) + \frac{cf}{d}\frac{ad}{(ad+bc)e}(ex_{10} - fx_{20}) = 0\end{aligned} \tag{2.28}$$

Thus, $\dot{V}$ is negative semi-definite $\forall x$.

The system converges towards the set $E = \{x \colon \dot{V} = 0\} = \{x = [x_1^*, x_2^*, x_3^*]^T\}$, and the infected equilibrium is the only invariant set contained in E. For this reason, applyling La Salle's theorem one can conclude that this equilibrium is locally asymptotically stable.

Also, since $x_3 = 0$ is the stable manifold for the virus-free equilibrium, one can conclude that the infected equilibrium is asymptotically stable $\forall x_3 > 0$. □

2.3 Phase portrait

In this section the phase portrait of the system is presented, obtained considering for each parameter the nominal value as defined in Table (1.1).

The phase portrait is reported in Figure 2.1. In the figure, system's trajectories from different starting conditions has been considered.

These initial conditions have been chosen considering the healthy range for the CD4/CD8 ratio, that is a useful indicator for the current state of the infection: in an healthy individual this ratio tipically varies in the range $[1.2; 2.2]$.

In particular:

- The yellow trajectory starts from the nominal healthy condition, i.e., $x_1(0) = x_{10}$, $x_2(0) = x_{20}$, with an initial viral load equal to $x_3(0) = 0.0001$ (that is, 1000 copies per ml).

- The purple trajectory starts from a low value of CD4 cells, equal to $x_1(0) = 500$, and a ratio CD4/CD8 equal to 2.2, so $x_2(0) = 318$; again, $x_3(0) = 0.0001$.

- The green trajectory starts from a high initial CD4 count $x_1(0) = 1500$, and CD4/CD8 equal to 1.2, so $x_2(0) =$; again, $x_3(0) = 0.0001$.

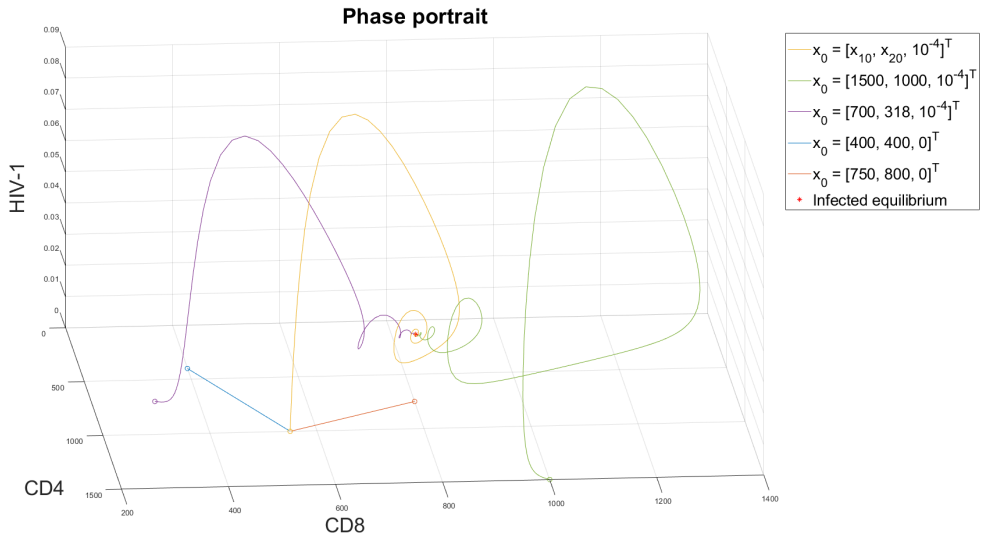

Figure 2.1: Phase portrait of the system.

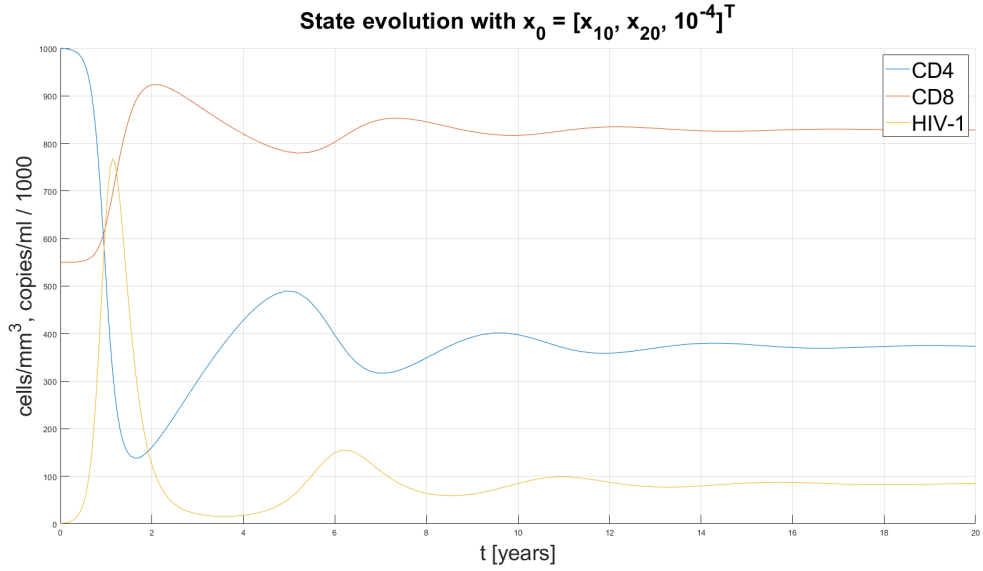

Figure 2.2: Full state evolution

Also, other two initial virus-free condition has been considered for the sake of completeness: the blue trajectory starting from $x(0) = [400, 400, 0]^T$ and the red trajectory starting from $x(0) = [750, 800, 0]^T$: notice how both converges to the nominal lymphocytes population $[x_{10}, x_{20}, 0]^T$.

As clarified by the portrait, the virus-free condition is unstable: even a small amount of viral load, without proper therapy, lead to the complete evolution of the infection. On the contrary, in a virus-free organism the lymphocytes population converges towards to nominal values.

Moreover, the focus-type dynamics of the infected equilibrium is clearly shown: the trajectories present significant oscillations, while being attracted to the equilibrium point. This behaviour can also be analyzed in Figures 2.3, 2.4 and 2.5, in which the three orthogonal views of the phase portrait are presented.

In Figure 2.6, the evolution of the CD4/CD8 ratio is presented for the three considered trajectories. The red striped lines represent the healthy range: even in the best case, after only 1.5 years the ratio falls below the minimum threshold. In all the cases, it stabilizes on a value of circa 0.45 after 15 years.

Finally, in Figure 2.2 the full system's state evolution is presented, with reference to the trajectory starting from the nominal lymphocytes count: $x(0) = [x_{10}, x_{20}, 0.0001]^T$.

This evolution is coherent with the available information currently known about the HIV infection dynamics [1].

During the primary phase, a large amount of cells in the body are rapidly infected, which leads to high levels of viral load measured in the blood. In the simulation, this phase corresponds to the first two years.

The viral load then drops to almost undetectable levels, since a virus-specific immunity is developed by the immunitary system. Nevertheless, it is known that HIV replication continues undetected, involving other tissues as the nervous system, that acts as hidden reservoirs of virus. This makes complete eradication of the virus impossible with currently available therapies.

2.3.1 The case $ex_{10} - fx_{20} < 0$

The phase portrait previously considered has been realized with reference to the case $\alpha = ex_{10} - fx_{20} > 0$, that is the typical scenario in practical applications.

For the sake of completeness, in Figure 2.7 one simulation obtained for $\alpha < 0$, starting from the initial condition $x(0) = [x_{10}, x_{20}, 0.05]^T$ is presented.

As stated in Section 2.1, in this case only the virus-free equilibrium exists, and any initial viral load is completely annihilated by the immunitary system's response.

The simulations have been carried out considering the nominal value for the parameter e, and a value of $f = 0.2 \Rightarrow \alpha = -1 < 0$.

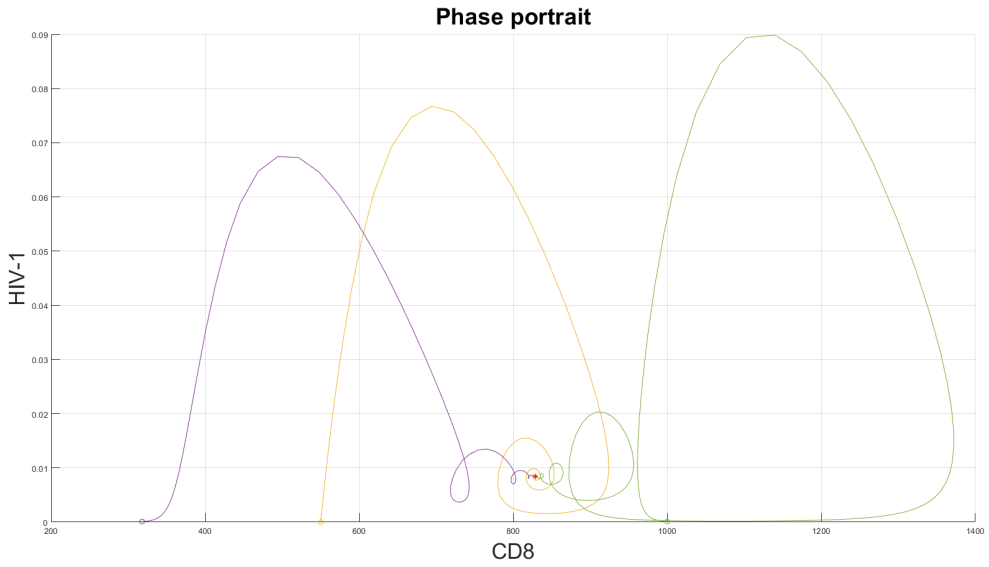

Figure 2.3: HIV-1 - CD8 evolution.

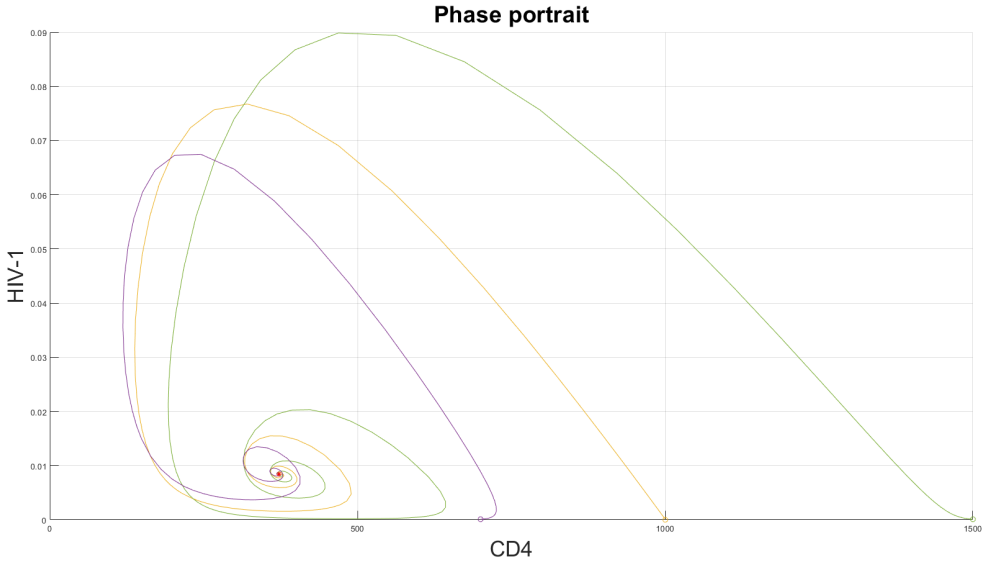

Figure 2.4: HIV-1 - CD4 evolution.

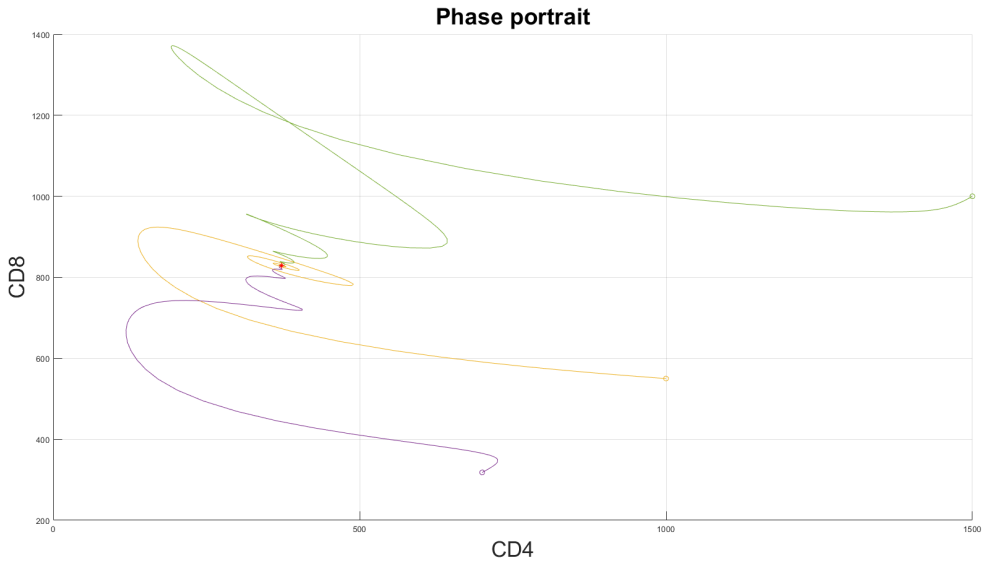

Figure 2.5: CD4 - CD8 evolution.

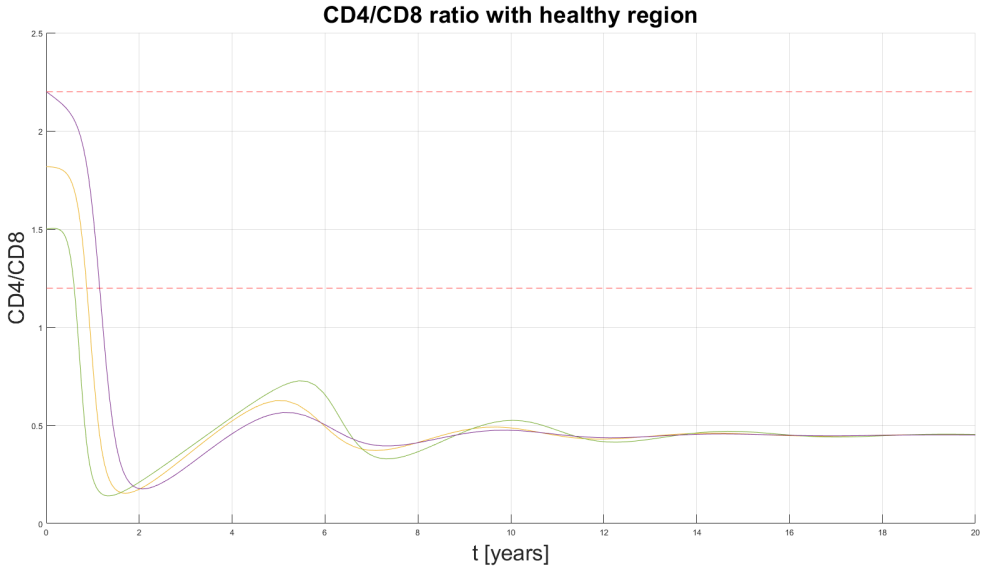

Figure 2.6: CD4/CD8 ratio and its healthy range.

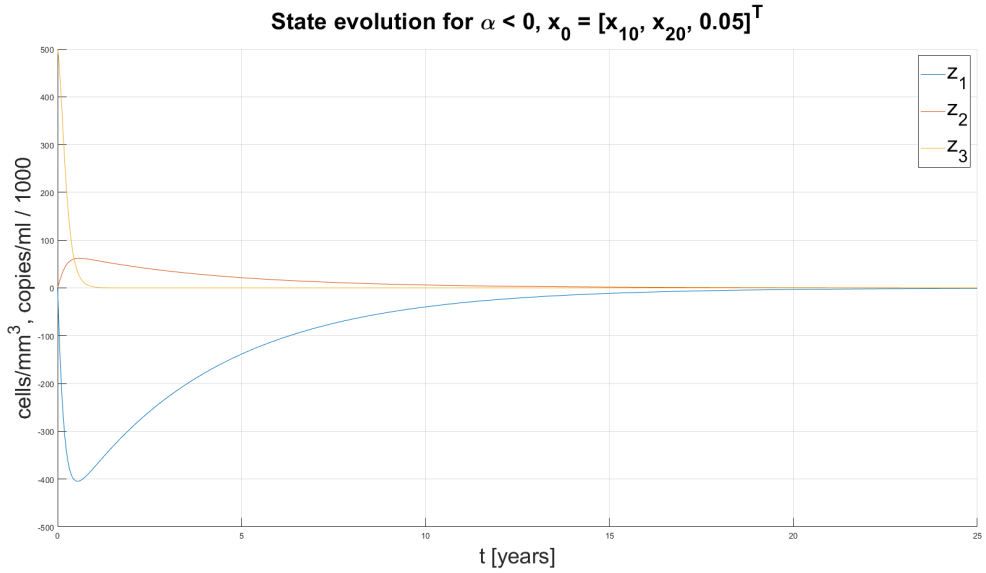

Figure 2.7: State evolution in the case $\alpha < 0$.

2.4 Bifurcation analysis

In this section, a bifurcation analysis of the system is performed.

In Section 2.1 the equilibria of the system and their stability properties has been studied. In particular, it has been found that:

- If $\alpha < 0$, the system has only one stable equilibrium (i.e., the virus-free condition)
- If $\alpha > 0$, the system has two equilibria:
  - the virus-free equilibrium, that is now an unstable equilibrium
  - the infected equilibrium, that is stable

It is clear that the parameter α plays a crucial role in the system's dynamics.

This can be interpreted as a transcritical bifurcation: the system has two equilibria, that exchange their stability properties when the system undergoes the bifurcation.

In particular, if $\alpha < 0$ the infected equilibrium would be unstable and characterized by a viral load $x_3 < 0$: this has no sense, since the state variables represent non-negative quantities. For this reason, the system presents only one equilibrium for $\alpha < 0$.

This analytical and intuitive discussion is now sustained by the following numerical analysis. In Figure 2.8 the bifurcation diagram for x_3, obtained using the MATCONT continuation software, is presented.

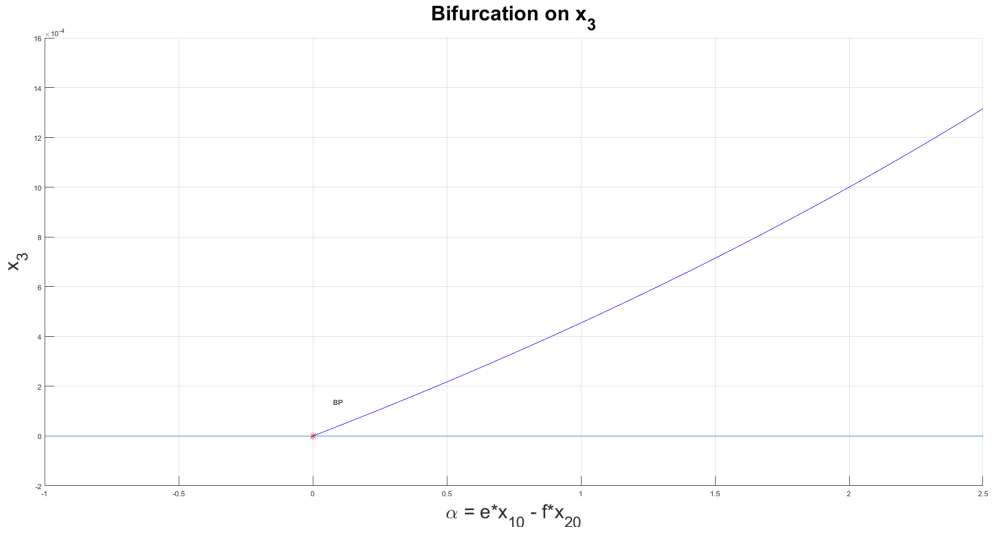

Figure 2.8: Bifurcation diagram for x_3.

When $\alpha = 0$, the software found a bifurcation point: it is represented in the figure by the name `BP`; starting from this point another branch bifurcates, and it is characterized by $x_3 = 0$.

Looking at the eigenvalues of the system in the two branches, the branch $x_3 = 0$ is stable for $\alpha < 0$ and unstable for $\alpha > 0$. This proves the correctness of the previous analysis.

In Figures 2.9 and 2.10 the bifurcation diagram for x_1 and x_2 are presented, too.

2.4.1 Transcritical bifurcation: normal form

In the previous section, it has been said that the system has a transcritical bifurcation in $\alpha = 0$ and $z_3 = x_3 = 0$.

For the Center Manifold Theorem [3, p. 303], this means that in a neighbourhood of the point $(z_3, \alpha) = (0, 0)$, the system's dynamics is topologically equivalent to the normal form:

$$\dot{\xi} = \eta\xi - \xi^2 \tag{2.29}$$

In this section, this equivalence will be proved.

Consider the system's equations (1.9). Since the parameter α has been defined as $\alpha = ex_{10} - fx_{20}$, we can write f as:

$$f = \frac{ex_{10} - \alpha}{x_{20}} \tag{2.30}$$

In this way, the system can be rewritten with explicit dependence from α. In particular, only the third equation changes to:

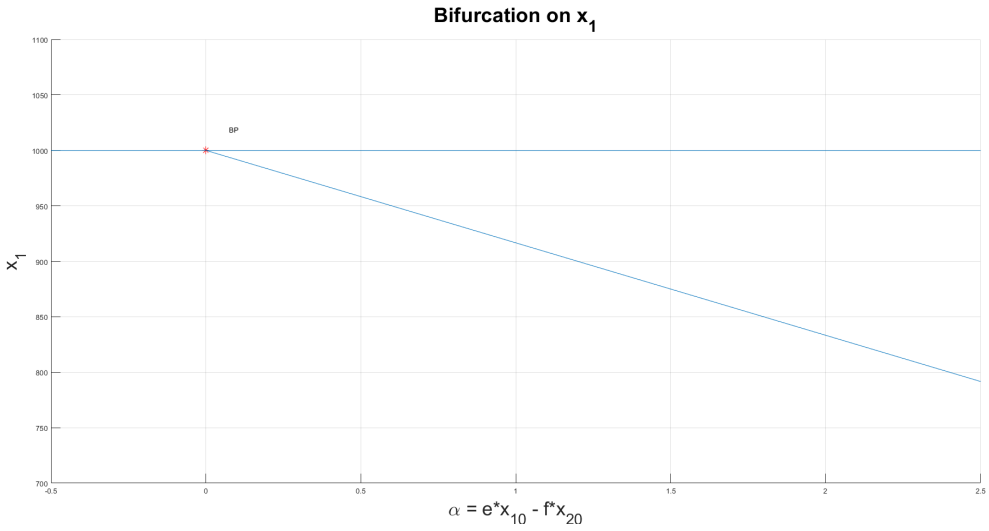

Figure 2.9: Bifurcation diagram for x_1.

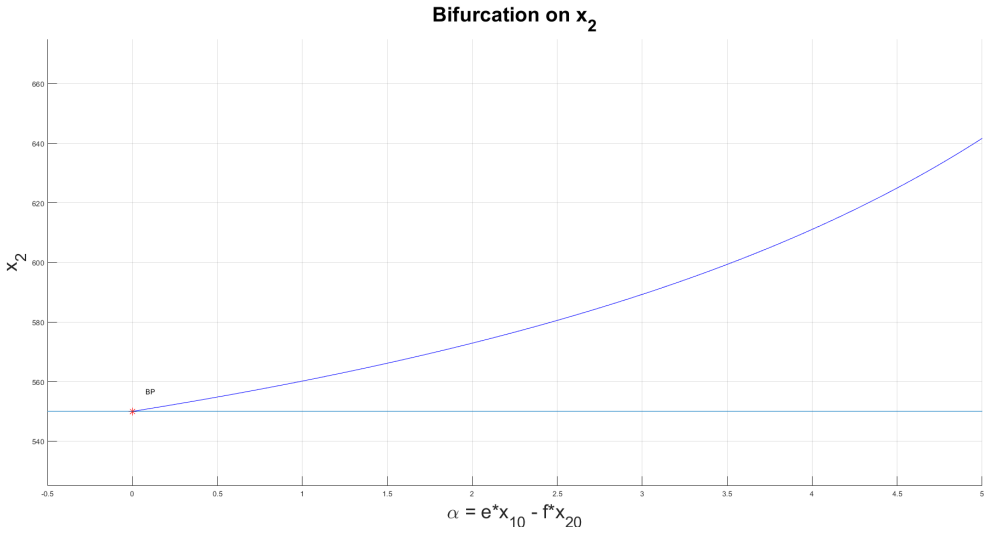

Figure 2.10: Bifurcation diagram for x_2.

$$\dot{z}_3 = z_3\Big[e(z_1 + x_{10}) + \frac{\alpha - ex_{10}}{x_{20}}(z_2 + x_{20})\Big] \tag{2.31}$$

The system's bifurcation point is $(z, \alpha) = (0, 0)$.

Linearizing the system, we get that:

$$\frac{\partial f(z)}{\partial z} = \begin{bmatrix} -a - bz_3 & 0 & -bz_1 \\ 0 & -c + dz_3 & dz_2 \\ ez_3 & -fz_3 & ez_1 - fz_2 \end{bmatrix}_{z=0} = \begin{bmatrix} -a & 0 & 0 \\ 0 & -c & 0 \\ 0 & 0 & 0 \end{bmatrix} \tag{2.32}$$

The eigenvalues and corresponding eigenvectors are:

$$\lambda_1 = -a \qquad v_1 = (1, 0, 0)^T \tag{2.33}$$

$$\lambda_2 = -c \qquad v_2 = (0, 1, 0)^T \tag{2.34}$$

$$\lambda_3 = 0 \qquad v_3 = (0, 0, 1)^T \tag{2.35}$$

Thus, the system is already in diagonal form, and no change of coordinates is needed.

We want to project the system's dynamics into the center manifold defined by z_3 and α. Define:

$$z_1 = h_1(z_3, \alpha) = a_0 + a_1 z_3 + a_2\alpha + a_3 z_3^2 + a_4\alpha^2 + a_5 z_3\alpha + O(\|(z_3, \alpha)\|^3) \tag{2.36}$$

$$z_2 = h_2(z_3, \alpha) = b_0 + b_1 z_3 + b_2\alpha + b_3 z_3^2 + b_4\alpha^2 + b_5 z_3\alpha + O(\|(z_3, \alpha)\|^3) \tag{2.37}$$

If $z_3 = 0$ and $\alpha = 0$, then also $z_1 = z_2 = 0$, and thus $a_0 = b_0 = 0$.

The time derivative $\dot{z}_1$ can be computed both directly from the model or differentiating Equation (2.36), and the same applies for $\dot{z}_2$.

Computing the time derivatives and equating the coefficients, the expression of h_1 and h_2 can be found.

Consider $\dot{z}_1$ first. Substituting Equations (2.36) and (2.37) into the system model yields:

$$\begin{aligned} \dot{z}_1 = -az_1 - b(z_1 + x_{10})z_3 = \\ = -(aa_1 + bx_{10})z_3 - aa_2\alpha - (aa_3 + ba_1)z_3^2 - aa_4\alpha^2 - \\ (aa_5 + ba_2)z_3\alpha + O(\|(z_3, \alpha)\|^3) \end{aligned} \tag{2.38}$$

Differentiating Equation (2.36) with respect to time and considering $\dot{\alpha} = 0$, yields:

$$\dot{z}_1 = \frac{\partial h_1(z_3,\alpha)}{\partial z_3}\dot{z}_3 + \frac{\partial h_1(z_3,\alpha)}{\partial \alpha}\dot{\alpha} = \frac{\partial h_1(z_3,\alpha)}{\partial z_3}\dot{z}_3 \tag{2.39}$$

where:

$$\frac{\partial h_1(z_3,\alpha)}{\partial z_3} = a_1 + 2a_3 z_3 + a_5\alpha \tag{2.40}$$

The time derivative $\dot{z}_3$ can be computed substituting Equations (2.36) and (2.37) into Equation (2.31):

$$\dot{z}_3 = e\Big(a_1 - \frac{x_{10}}{x_{20}}b_1\Big)z_3^2 + e\Big(a_2 - \frac{x_{10}}{x_{20}}b_2 + 1\Big)z_3\alpha + O(\|(z_3,\alpha)\|^3) \tag{2.41}$$

Equating coefficients of the same terms from Equations (2.38) and (2.39) yields:

$$a_1 = -\frac{b}{a}x_{10} \tag{2.42}$$

$$a_2 = 0 \tag{2.43}$$

$$a_3 = \frac{1}{a}\Big(e\frac{x_{10}}{x_{20}}a_1 b_1 - e a_1^2 - b a_1\Big) \tag{2.44}$$

$$a_4 = 0 \tag{2.45}$$

$$a_5 = \frac{1}{a}\Big(e\frac{x_{10}}{x_{20}}b_2 - 1\Big) \tag{2.46}$$

Following the same steps for h_2 and computing the parameters, we finally get:

$$z_1 = h_1(z_3,\alpha) = -\frac{b}{a}x_{10}z_3 + a_3 z_3^2 - \frac{1}{a}z_3\alpha + O(\|(z_3,\alpha)\|^3) \tag{2.47}$$

$$z_2 = h_2(z_3,\alpha) = +\frac{d}{c}x_{20}z_3 + b_3 z_3^2 + \frac{1}{c}z_3\alpha + O(\|(z_3,\alpha)\|^3) \tag{2.48}$$

$$\tag{2.49}$$

where:

$$a_3 = -\frac{b}{a^2}x_{10}\Big(\frac{bce + ade}{ac}x_{10} - b\Big) \tag{2.50}$$

$$b_3 = +\frac{d}{c^2}x_{20}\Big(\frac{bce + ade}{ac}x_{10} + d\Big) \tag{2.51}$$

$$\tag{2.52}$$

Now, substituting the expressions (2.47) and (2.48) in Equation (2.31):

$$\begin{aligned}\dot{z}_3 &= z_3\alpha - \frac{bce+ade}{ac}x_{10}z_3^2 + O(\|(z_3,\alpha)\|^3) \\ &= z_3\alpha - kz_3^2 + O(\|(z_3,\alpha)\|^3)\end{aligned} \tag{2.53}$$

where $k = -\frac{bce+ade}{ac}x_{10}$.

Finally, letting $\eta = \alpha$, $\xi = kz_3$ and differentiating with respect to time yields:

$$\begin{aligned}\dot{\xi} &= k\dot{z}_3 = \\ &= kz_3\alpha - k^2z_3^2 + O(\|(z_3,\alpha)\|^3) = \\ &= \eta\xi - \xi^2 + O(\|(\xi,\eta)\|^3)\end{aligned} \tag{2.54}$$

So, the system's dynamics in a neighbourhood of the bifurcation point is topologically equivalent to the normal form of the transcritical bifurcation.

Chapter 3

Control

In this chapter, the control problem of the system is tackled.

Consider the system's equations (1.9). The growth of the HIV-1 population is obstructed by the external control agent u; the system's equations become:

$$\begin{cases} \dot{z}_1 &= -az_1 - b(z_1 + x_{10})z_3 \\ \dot{z}_2 &= -cz_2 + d(z_2 + x_{20})z_3 \\ \dot{z}_3 &= z_3[e(z_1 + x_{10}) - f(z_2 + x_{20})] - u \end{cases} \tag{3.1}$$

The viral load can be considered as the output of the system:

$$y = \begin{bmatrix} 0 & 0 & 1 \end{bmatrix} z \tag{3.2}$$

Any designed control strategy needs to stabilize the state to zero, satisfying the non-negative properties of the original system, and limit the control effort.

With the current international recommendations, an effective HAART therapy should decrease the viral load to a value $x_3 < 50$ copies/ml within 12 months circa of treatment. Under this threshold, the infection is **non-communicable** (see [6]). If this is not the case, the treatment has failed.

Remember that the control agent u is obtained through a combination of different antiretroviral agents, that can cause adversal effects.

Deriving the actual correspondence between the medication and the control agent value is outside the scope of this paper. However, the control will always be considered with the minimum possible value as to reach the non-communicable threshold as specified before, so to minimize the adversal effects.

Moreover, notice that in the practical case, a continuous control is not possible; the lymphocytes population and viral load are sampled in a periodic fashion, and therapies are modified accordingly to the measured values. In this paper, the controller will be discretized using a zero-order hold, with a sampling time $T_s = 1$ week.

In all the following control approaches, the simulations of the nonlinear system will be carried out with the initial condition $x_0 = [950, 550, x_3(0)]^T$, where the initial viral load is $x_3(0) = 0.0006$ cells/mm^3 = 6000 copies/ml.

In this chapter, three different controllers will be designed. First, the control of the linearized model near the virus-free equilibrium will be considered; then, the feedback linearization approach will be used to control the non-linear system. Finally, since in practice it can be difficult to measure the model parameters (in particular e and f [1]) this controller will be empowered by an adaptive law to cope with this uncertanty.

Each control scheme will be derived in a separate section, and a numerical simulation of the control performances in the ideal case is presented. Finally, in Section 3.4, a comparison between the controllers is considered, also taking into account non-idealities like parameter uncertanties and noise.

The performances achieved with these controllers will be discussed and compared, with a focus on the following aspects:

- Convergence of the viral load under the non-communicable threshold of 50 copies/ml, and the time required to do so.
- Maximum value of the control action.
- Robustness with respect to parameter uncertanties on e and f.
- Robustness with respect to measurement noise, modeled as a white noise, that approximates the possible variation of blood analysis results.

Notice that the control schemes designed in this paper cannot be directly used in practice when the viral load is under the measurable threshold of 50 copies/ml (20 copies/ml with new techniques). Instead, a milder long-term drug therapy could be prescribed as well as periodic monitoring of the patient condition.

3.1 Control based on the linearized system

In this section a linear control strategy is designed, with reference to the linearized model of the system in a neighbourhood of the virus-free equilibrium; the designed control is then applied to the nonlinear model, and its performances analyzed.

The linearization of the system around the virus-free equilibrium, defined in Equation (2.1), can be easily written starting from the Jacobian matrix found in Equation (2.3). The linearized system around the equilibrium is described by:

$$\delta \dot{z} = \begin{bmatrix} -a & 0 & -bx_{10} \\ 0 & -c & dx_{20} \\ 0 & 0 & ex_{10} - fx_{20} \end{bmatrix} \delta z + \begin{bmatrix} 0 \\ 0 \\ -1 \end{bmatrix} u \tag{3.3}$$

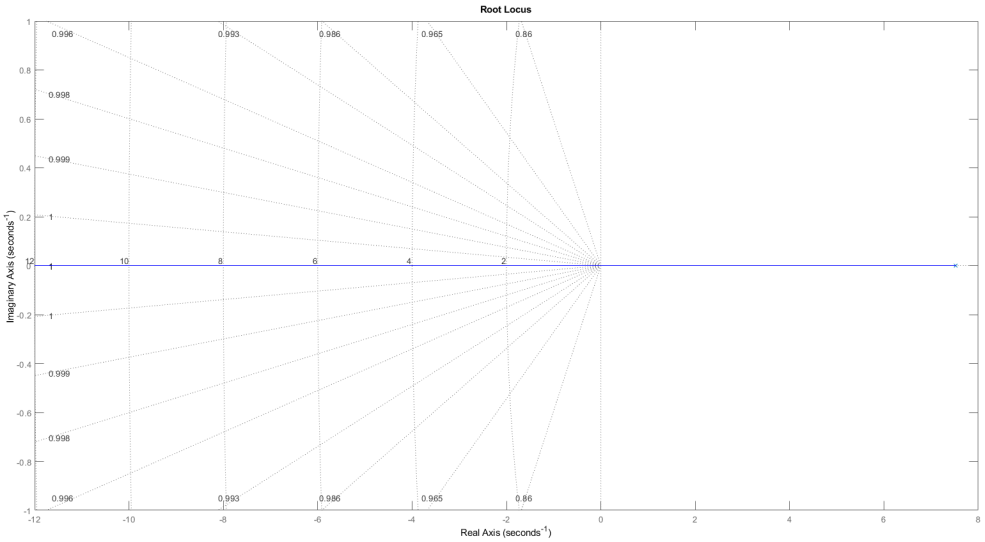

Figure 3.1: Root locus

Now, we can use any classical control strategy for linear system. Assuming that the viral load is measurable, the simplest choice is to adopt a proportional control law, using an output feedback scheme.

In particular, since the control u enters in the B matrix with negative sign, one can select:

$$u = -ke_{\text{rr}} = kz_3, \qquad k > 0 \tag{3.4}$$

where the error is defined as $e_{\text{rr}} = r - z_3 = -z_3$, obtained considering a null reference value.

With thoise choice, the eigenvalues of the system are:

$$\lambda_1 = -a < 0, \qquad \lambda_2 = -c < 0, \qquad \lambda_3 = ex_{10} - fy_{10} - k \tag{3.5}$$

Choosing the control gain such that:

$$k > ex_{10} - fy_{10} \tag{3.6}$$

leads to $\lambda_3 < 0$, and thus the local stability of the controlled system around the healthy equilibrium point is guaranteed.

This is the same as considering the root locus of the system, reported in Figure 3.1: the locus crosses the imaginary axis for $k = ex_{10} - fy_{10}$, and the system has a real negative pole for any k greater than this value.

Notice that, for this controller, only the viral load must be measured.

The control scheme is presented in Figure 3.2.

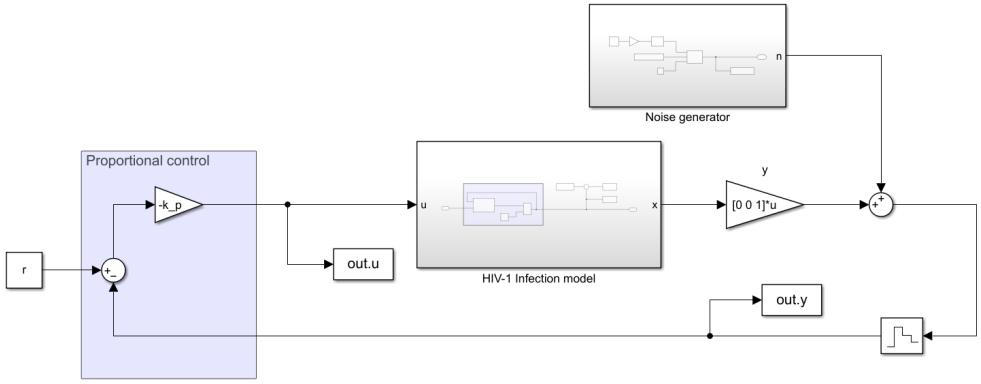

Figure 3.2: Linear control scheme.

3.1.1 Numerical simulation

Consider the non-linear system under the action of the purely proportional control, in absence of any noise and disturbance.

The initial condition has been chosen as $x_0 = [950, 550, 0.0006]^T$; the control gain has been selected as $k = 11.45$.

The control action and system's states evolution are presented in Figure 3.4.

The controller is able to stabilize the system, having x_1 and x_2 tend to their nominal value x_{10} and x_{20}, and the viral load to zero. In particular, the viral load drops under the non-communicable threshold after 11.54 months, less than a year: thus, the treatment is considered successful. The settling time at 5% of the CD4 population to its nominal value is $t_{s,5\%} = 12.35$ years.

Also, the control action has a maximum initial peak equal to $\max u = 0.00687$. Remember that a smaller value of the control action corresponds to less adversal effects for the patient.

In Figure 3.3 a zoom of the viral load evolution is presented, highlighting the crossing of the 50 copies/ml threshold.

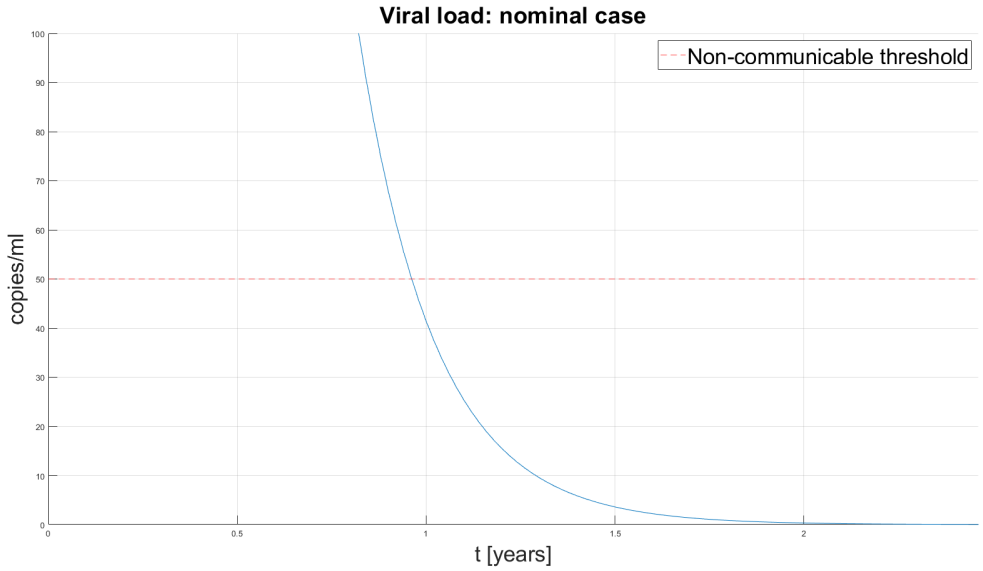

Figure 3.3: Viral load goes under the non-communicable threshold, using proportional controller.

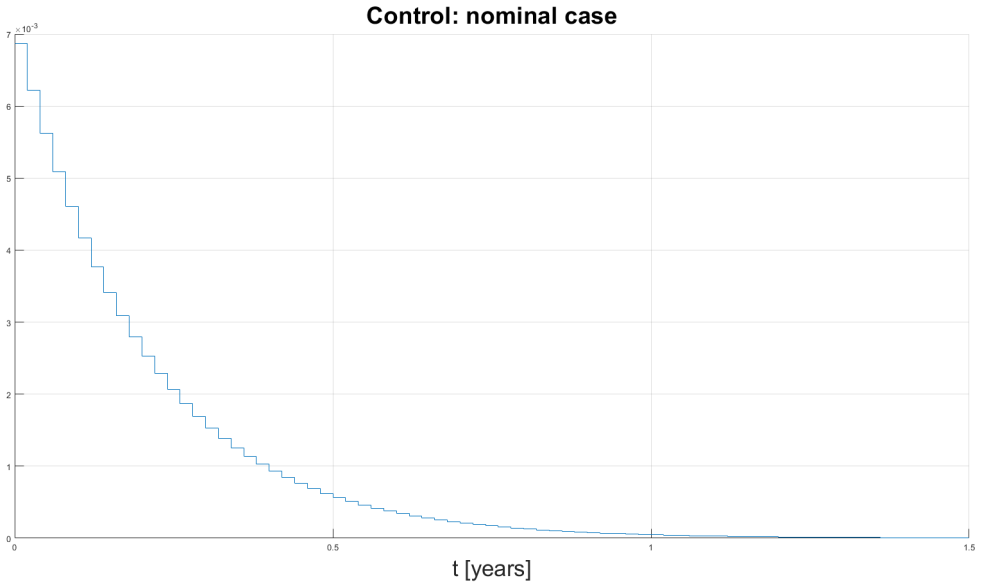

(a) *Control action.*

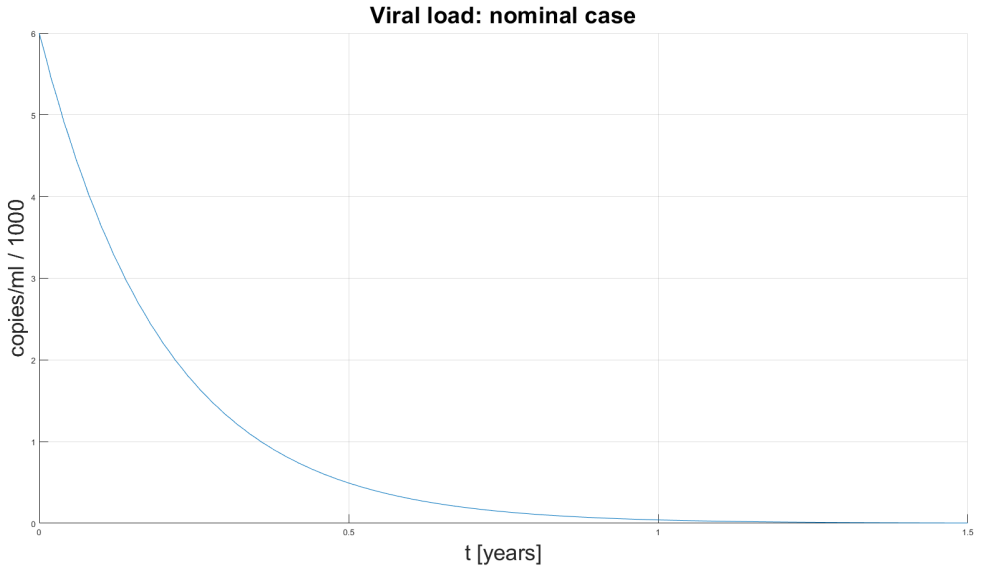

(b) *Viral load evolution.*

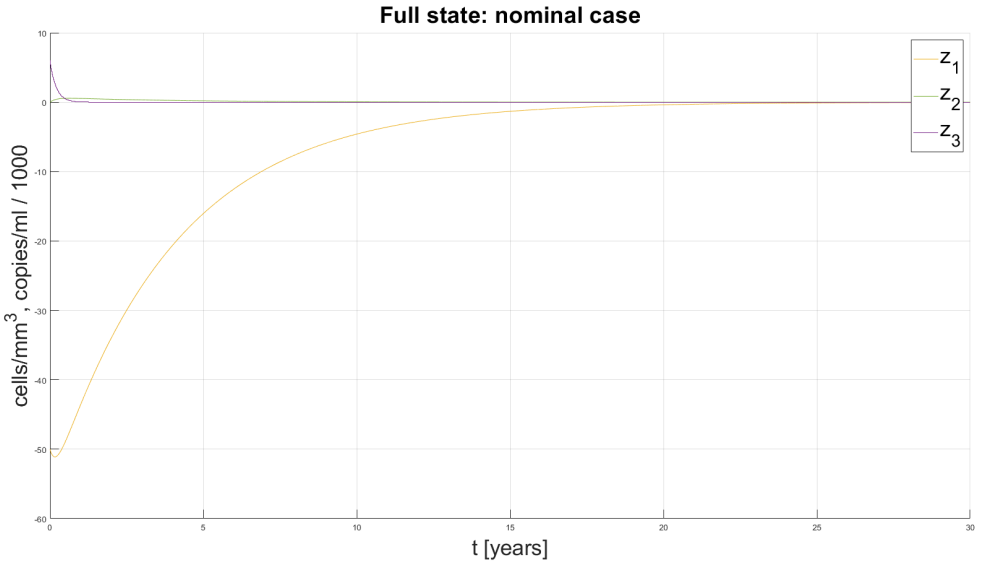

(c) *System's state evolution.*

Figure 3.4: Proportional controller performances in the nominal case.

3.2 I/O feedback linearization

In this section, an input-output feedback linearization control approach is considered; the designed control is then applied to the nonlinear model, and its performances analyzed.

Consider the system's equations (3.1). If we assume $y = z_3$ as the output of the system, the time derivative of first order is:

$$\dot{y} = \dot{z}_3 = z_3[e(z_1 + x_{10}) - f(z_2 + x_{20})] - u$$

In order to linearize the y dynamics, we can simply choose:

$$u = z_3[e(z_1 + x_{10}) - f(z_2 + x_{20})] - v \tag{3.7}$$

This choice lead to the equation $\dot{y} = v$. Thus, one can control the output dynamics by choosing an opportune control law v. For example, considering:

$$v = -ky = -kz_3 \tag{3.8}$$

the closed-loop system's output dynamics is governed by the equation:

$$\dot{z}_3 + kz_3 = 0 \tag{3.9}$$

and so the viral load tends to zero, with a velocity that depends on the choice of the control gain k.

Notice that, in order to implement this controller, one needs to measure the whole system's state, and not only the viral load as for the linear proportional controller.

The time derivative $\dot{y} = \dot{z}_3$ has a direct dependance from the control input u, and thus the system has a relative degree $m = 1 < 3$. This means that we have two internal dynamics, i.e., $\dot{z}_1$ and $\dot{z}_2$, and we must ensure that these dynamics are stable.

Theorem 6. *Under the feedback linearization control law (3.7), in case of perfect model knowledge, the virus-free equilibrium $z = 0$ is globally asymptotically stable for the system (3.1).*

Proof. Consider the following Lyapunov candidate function:

$$V = p_1\Big(x_1 - x_{10} - x_{10}\log\frac{x_1}{x_{10}}\Big) + p_2\Big(x_2 - x_{20} - x_{20}\log\frac{x_2}{x_{20}}\Big) + p_3x_3 \tag{3.10}$$

where $p_i > 0$, $i = 1, 2, 3$. As discussed in Section 2.2.1, this function is positive definite in the neighbourhood of the virus-free equilibrium.

Differentiating with respect to time, and assuming $\dot{x}_3 = -kx_3$, $k > 0$:

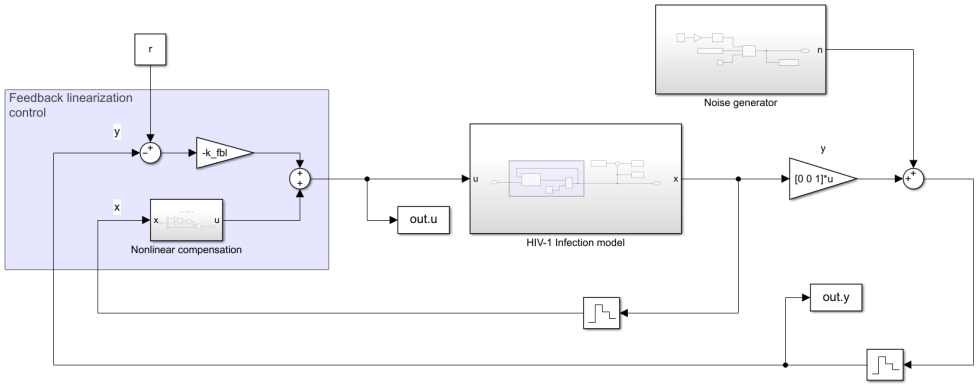

Figure 3.5: Feedback linearization control scheme.

$$\dot{V} = p_1 \frac{x_1 - x_{10}}{x_1}\dot{x}_1 + p_2 \frac{x_2 - x_{20}}{x_2}\dot{x}_2 + p_3\dot{x}_3 = \\ = -p_1 a \frac{(x_{10} - x_1)^2}{x_1} - p_2 c \frac{(x_{20} - x_2)^2}{x_2} \\ - [p_1 b(x_1 - x_{10}) - p_2 d(x_2 - x_{20}) + p_3 k]x_3 \quad (3.11)$$

Choosing $p_1 = (e/b)p_3$, $p_2 = (f/d)p_3$, and $p_3 = 1$, yields:

$$\dot{V} = -\frac{ae}{b}\frac{(x_{10} - x_1)^2}{x_1} - \frac{cf}{d}\frac{(x_{20} - x_2)^2}{x_2} - [e(x_1 - x_{10}) - f(x_2 - x_{20}) + k]x_3 \quad (3.12)$$

In order to have $\dot{V} < 0$ it should be $k > e(x_1 - x_{10}) - f(x_2 - x_{20})$.
For Theorem (2), it is $x_1 < x_{10}$ and $x_2 > x_{20}$; so one can write:

$$k > e(x_1 - x_{10}) - f(x_2 - x_{20}) \geq e(\max(x_1) - x_{10}) - f(\min(x_2) - x_{20}) = \\ = e(x_{10} - x_{10}) - f(x_{20} - x_{20}) = 0 \quad (3.13)$$

For this reason, $\dot{V}$ is negative definite $\forall k > 0$.
Also, the function V is radially unbounded: we can conclude that the virus-free equilibrium is globally asymptotically stable. □

The control scheme implemented in MATLAB is reported in Figure 3.5.

3.2.1 Numerical simulation

Consider the non-linear system under the action of the proposed feedback linearization control scheme in ideal conditions, i.e., in absence of any noise and disturbance.

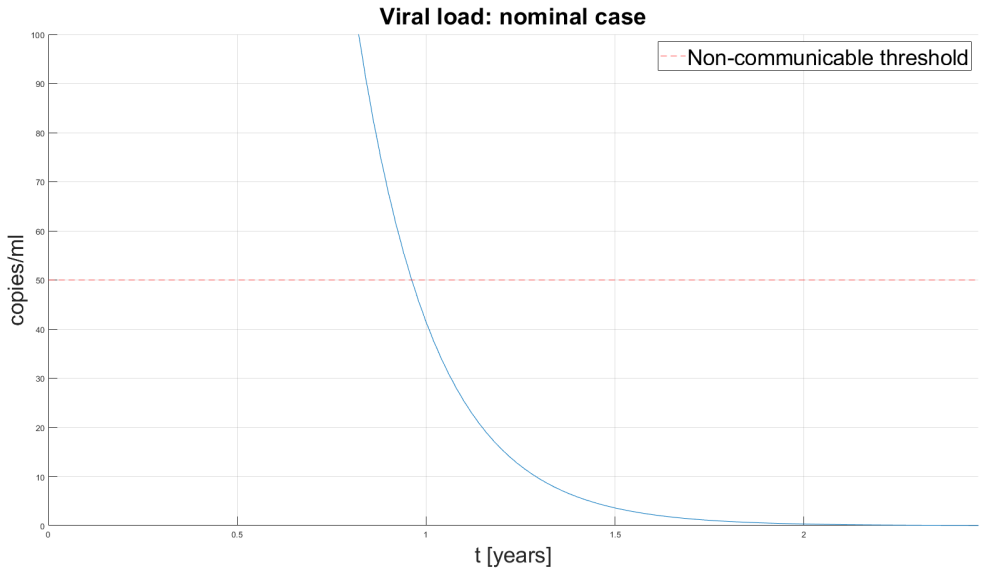

Figure 3.6: Viral load goes under the non-communicable threshold, using feedback linearization controller.

The initial condition has been chosen as $x_0 = [950, 550, 0.0006]^T$; the control gain has been selected as $k = 4.35$.

The control action and system's states evolution are presented in Figure 3.7. In Figure 3.6 a zoom of the viral load evolution is presented, highlighting the crossing of the 50 copies/ml threshold.

The controller is able to stabilize the system: in particular, the viral load drops under the detectable threshold after 11.74 months, thus the treatment is successful. The settling time at 5% of the CD4 population to its nominal value is $t_{s,5\%} = 12.36$ years.

The control action has a maximum initial peak equal to $\max u = 0.006825$.

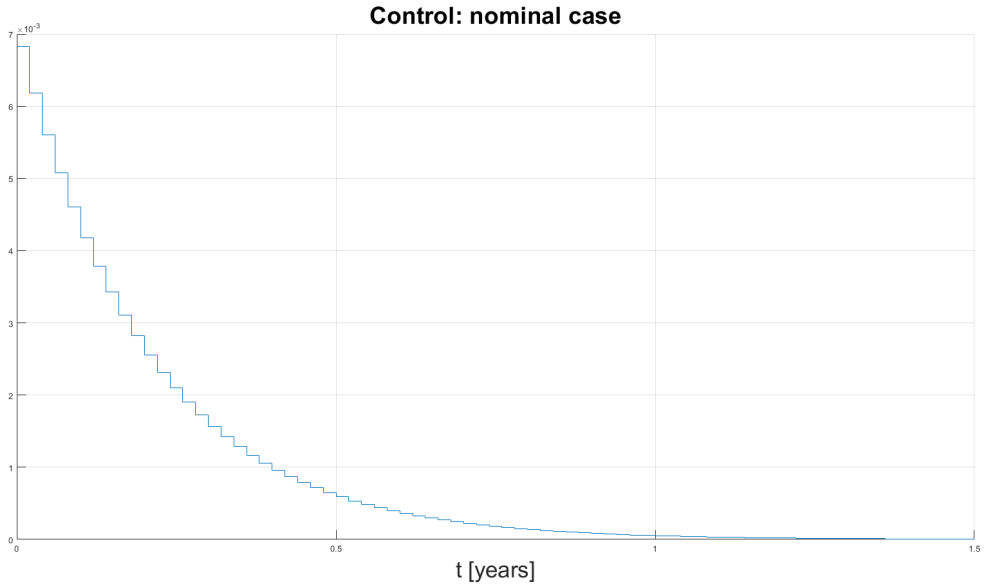

(a) *Control action.*

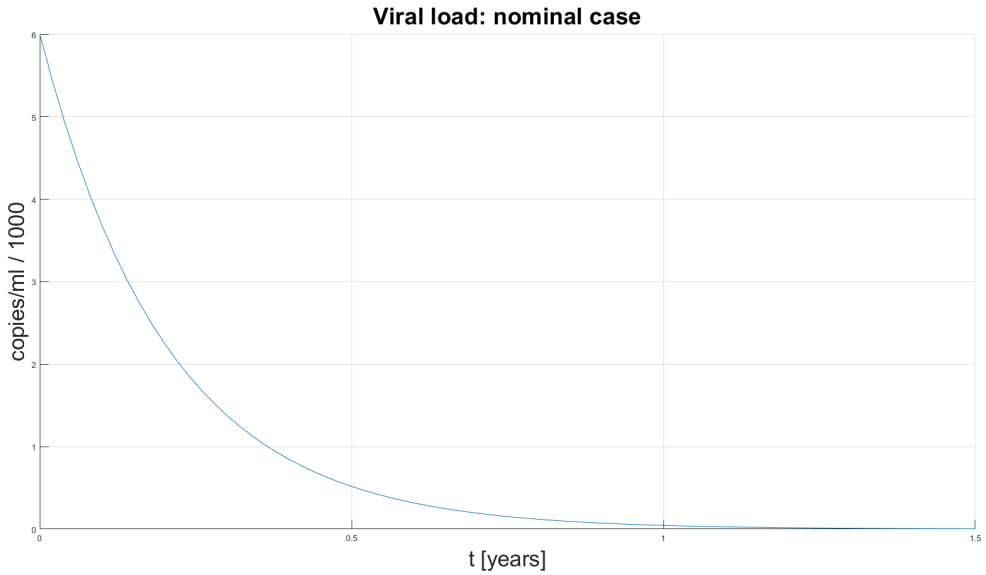

(b) *Viral load evolution.*

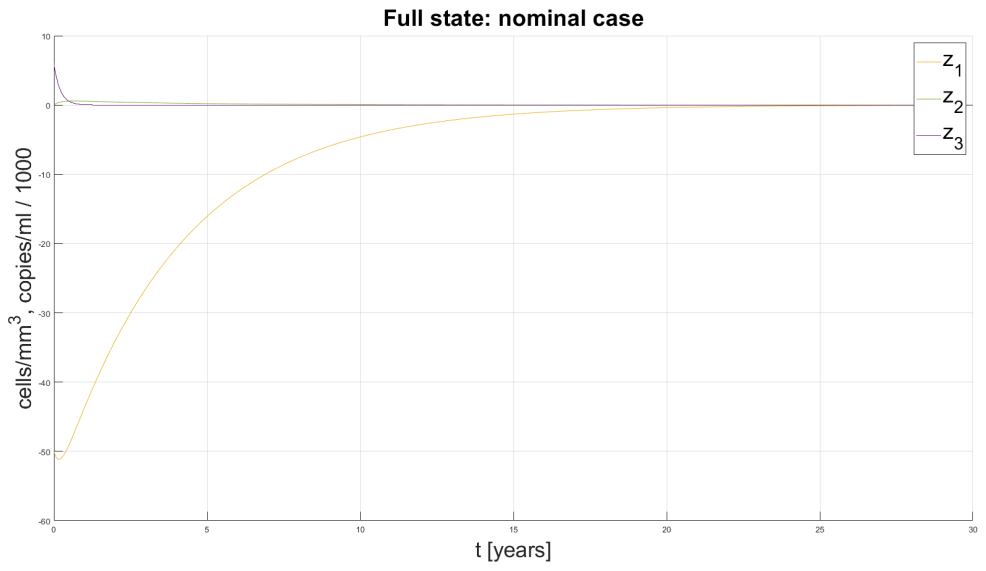

(c) *System's state evolution.*

Figure 3.7: Feedback linearization controller performances in the nominal case.

3.3 Adaptive control based on I/O feedback linearization

As discussed in [1], in practical scenarios it can be very difficult to obtain a correct estimation of the model parameters, in particular e and f.

It is well known in literature that the feedback linearization control scheme could suffer if the model is not perfectly known.

However, recalling the results obtained with the proportional controller in Section 3.1, it can be easily understood that the feedback linearization scheme could nullify the viral load if control gain is large enough; but, as said before, greater gains means heavier drug dosage and adversal effects.

For these reasons, a natural question that arise is if it's possible to robustify the feedback linearization scheme with respect to parameter uncertainties, and reduce the required control effort, introducing an adaptive control law for estimating e and f.

The adaptive extention of the feedback linearization scheme is designed as discussed in [4]: in particular, the adaptive law can be obtained by using the Lyapunov theory.

Consider the following reference model:

$$\begin{cases} \dot{z}_{3,m} &= -kz_{3,m} \\ y_m &= z_{3,m} \end{cases} \tag{3.14}$$

representing a linear dynamics for the output z_3; also, if the parameters e and f are not exactly known, the control law defined by Equation (3.7) and (3.8) can be rewritten as:

$$u = [\hat{e}(z_1 + x_{10}) - \hat{f}(z_2 + x_{20})]z_3 + kz_3 \tag{3.15}$$

where $\hat{e}, \hat{f}$ represents the estimate of e and f respectively.

Consider now the error:

$$e_{rr} = y - y_m \tag{3.16}$$

Differentiating with respect to time yields:

$$\dot{e}_{rr} = [\tilde{e}(z_1 + x_{10}) - \tilde{f}(z_2 + x_{20})]z_3 - ke_{rr} \tag{3.17}$$

where:

$$\tilde{e} = e - \hat{e}, \qquad \tilde{f} = f - \hat{f} \tag{3.18}$$

represent the estimation error.

Consider the following Lyapunov candidate function:

$$V = \frac{1}{2}e_{rr}^2 + \frac{1}{2\alpha}(\hat{e} - e)^2 + \frac{1}{2\beta}(\hat{f} - f)^2, \qquad \alpha, \beta > 0 \tag{3.19}$$

Clearly it is:

$$V \geq 0, \qquad \forall (e_{rr}, \hat{e}, \hat{f}) \in \mathbb{R}^3 \tag{3.20}$$

$$V = 0 \iff (e_{rr}, \hat{e}, \hat{f}) = (0, e, f) \tag{3.21}$$

Differentiating V with respect to time:

$$\dot{V} = e_{rr}\dot{e}_{rr} + \frac{1}{\alpha}(e - \hat{e})\dot{\hat{e}} + \frac{1}{\beta}(f - \hat{f})\dot{\hat{f}} =$$
$$- ke_{rr}^2 + (e - \hat{e})\Big(\frac{\dot{\hat{e}}}{\alpha} - (z_1 + x_{10})z_3 e_{rr}\Big) + (f - \hat{f})\Big(\frac{\dot{\hat{f}}}{\alpha} + (z_2 + x_{20})x_3 e_{rr}\Big) \tag{3.22}$$

Thus, choosing the adaptive control law as:

$$\begin{cases} \dot{\hat{e}} & = \alpha(z_1 + x_{10})z_3 e_{rr} \quad = \alpha x_1 x_3 e_{rr} \\ \dot{\hat{f}} & = -\beta(z_2 + x_{20})z_3 e_{rr} \quad = \beta x_2 x_3 e_{rr} \end{cases} \tag{3.23}$$

one gets $\dot{V} \leq 0$, and so the point $(e_{rr}, \hat{e}, \hat{f}) = (0, e, f)$ is a stable equilibrium point.

It is worth noticing that, while the error converges to zero, not necessarily $\hat{e}$ and $\hat{f}$ will converge to the real values e and f; however, they are bounded, and will reach some values such that $e_{rr} \to 0$.

The control scheme implemented in MATLAB is reported in Figure 3.8.

Notice that a gain locking algorithm has been implemented too, in order to avoid unbounded growth of the estimated parameters in presence of persistent disturbanes.

3.3.1 Numerical simulation

Consider the non-linear system under the action of the proposed adaptive control scheme, in absence of any noise and disturbance.

The initial condition has been chosen as $x_0 = [950, 550, 0.0006]^T$; the control gains has been selected as $k = 12$, $\alpha = \beta = 1 \cdot 10^{-5}$.

The control action and system's states evolution are presented in Figures 3.9 and 3.9, as well as the evolution of estimated parameters.

The controller is able to stabilize the system and, the viral load drops under the detectable threshold after 10.22 months, thus the treatment is successful. The settling time at 5% of the CD4 population to its nominal value is $t_{s,5\%} = 12.31$ years.

The control action has a maximum initial peak equal to $\max u = 0.0072$.

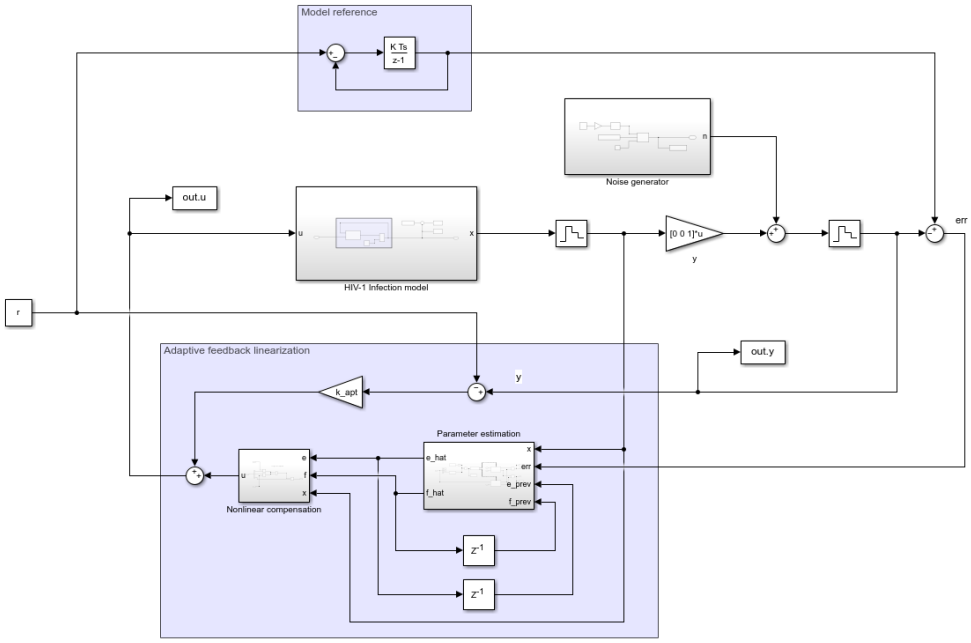

Figure 3.8: Adaptive control scheme.

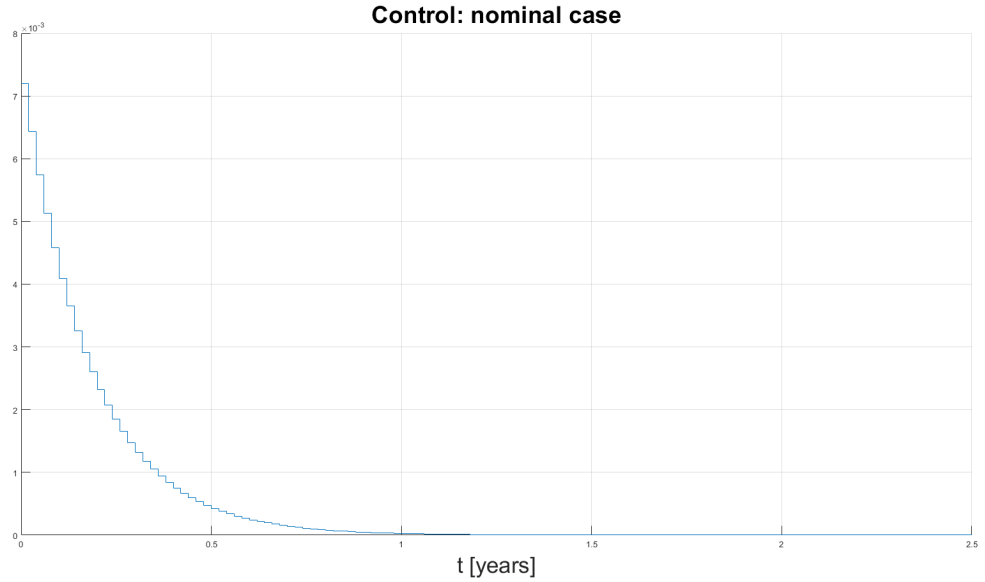

(a) *Control action.*

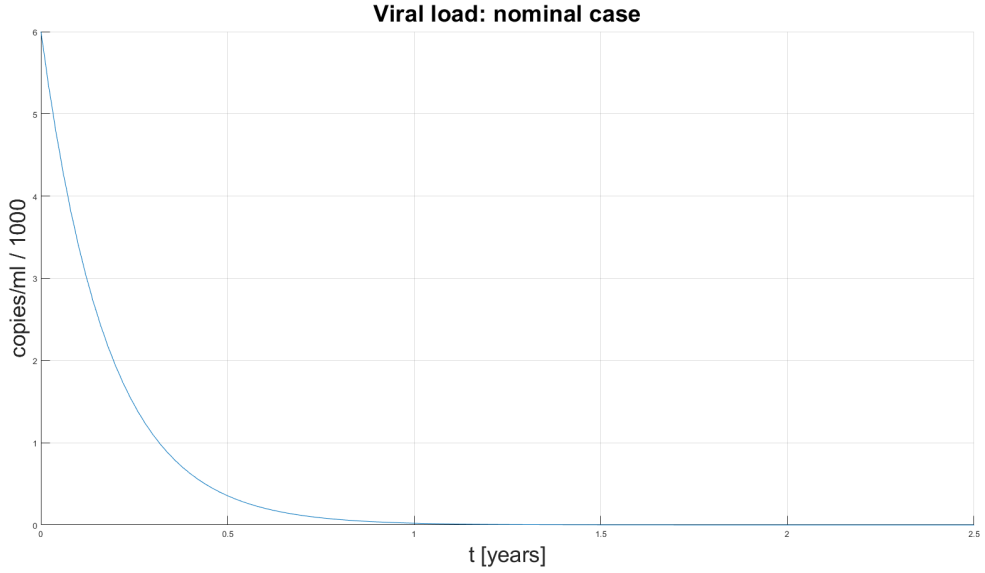

(b) *Viral load evolution.*

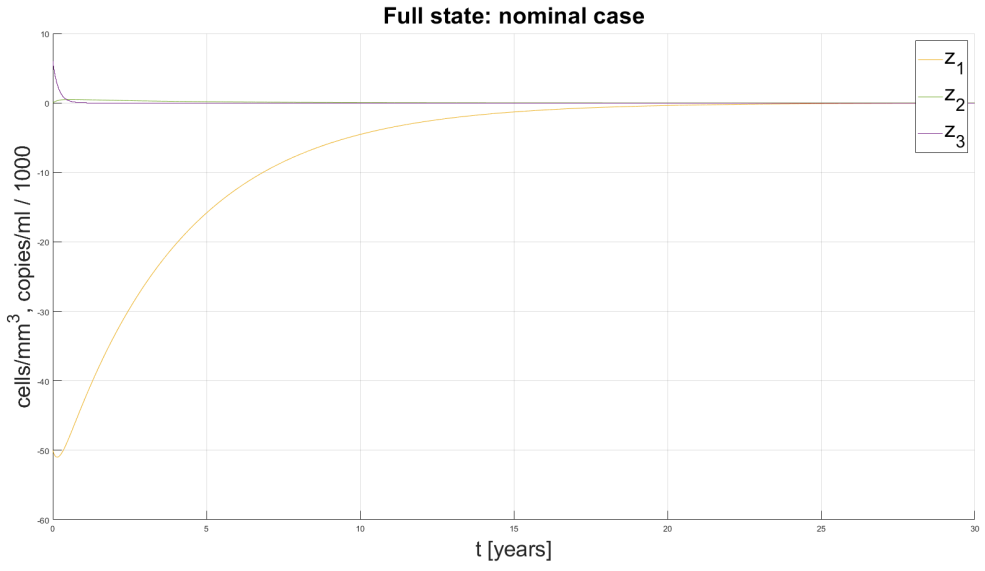

(c) *System's state evolution.*

Figure 3.9: Adaptive controller performances in the nominal case.

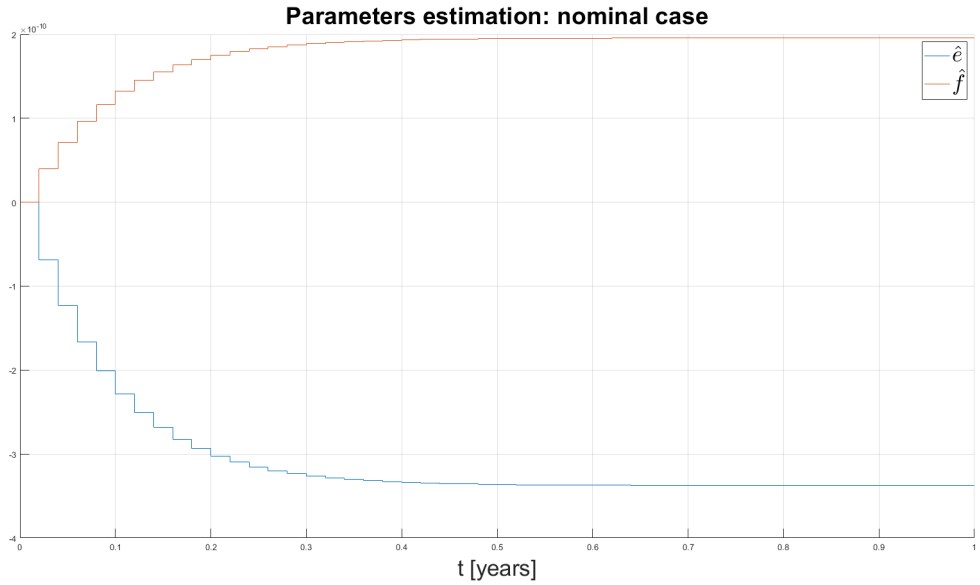

(a) *Parameter estimation.*

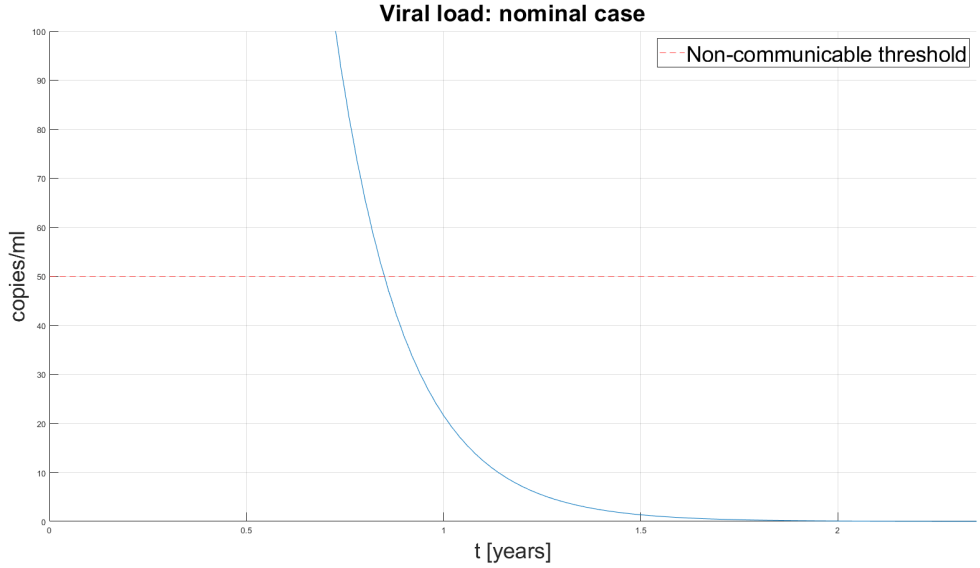

(b) *Viral load goes under the non-communicable threshold.*

Figure 3.10: Adaptive controller performances in the nominal case (continued).

Control strategy	Gains
Proportional	$k = 11.45$
Feedback linearization	$k = 4.35$
Adaptive	$k = 12$ $\alpha = \beta = 1 \cdot 10^{-5}$

Table 3.1: Control gains for different strategies.

3.4 Control comparison

In this section, a comparison between the linear and nonlinear controls developed in the previous sections is carried out. For all the controls and simulations, the system's initial condition has been chosen as $x(0) = [950, 550, 0.0006]^T$.

In order to have an in-depth comparison, the control performances will be evaluated with respect to the following scenarios:

- The nominal ideal case: all the model's parameters are perfectly known and no disturbance is applied.
- A 5% uncertainty is applied to the knowledge of e and f parameters, in the worst case scenario (e bigger and f smaller than the nominal value).
- A 35% uncertainty is applied to the knowledge of e and f, as the previous point.
- A white noise is applied to the measurement of the system's output, i.e., the viral load

The choices made for control gains under different control strategies have been summarized in Table (3.1).

3.4.1 Nominal scenario

Consider the ideal scenario, with perfect model knowledge and absence of any external disturbance.

All the three control schemes are able to stabilize the system and nullify the viral load.

In Figures 3.11 and 3.12 the evolution of the control action, system's state and parameter estimation is presented. The performances of the three controls are summarized in Table (3.2).

Each control scheme is able to achieve the desired performances, making the viral load goes under the non-communicable threshold in less than one year. In particular, the feedback linearization action is the slowest, requiring almost

Scheme	**Non-communicable time** [months]	**Steady state**	**Control peak** [$\cdot 10^{-3}$]
Proportional	11.54	virus-free	6.87
Feedback linearization	11.74	virus-free	6.62
Adaptive	10.22	virus-free	7.2

Table 3.2: Controls comparison in nominal scenario.

12 months to do so: however, this is compensated by the lowest control effort among the three. On the other end, the adaptive controller is the quickest, at the price of the largest control effort. The proportional scheme presents an intermediate behaviour between the other two.

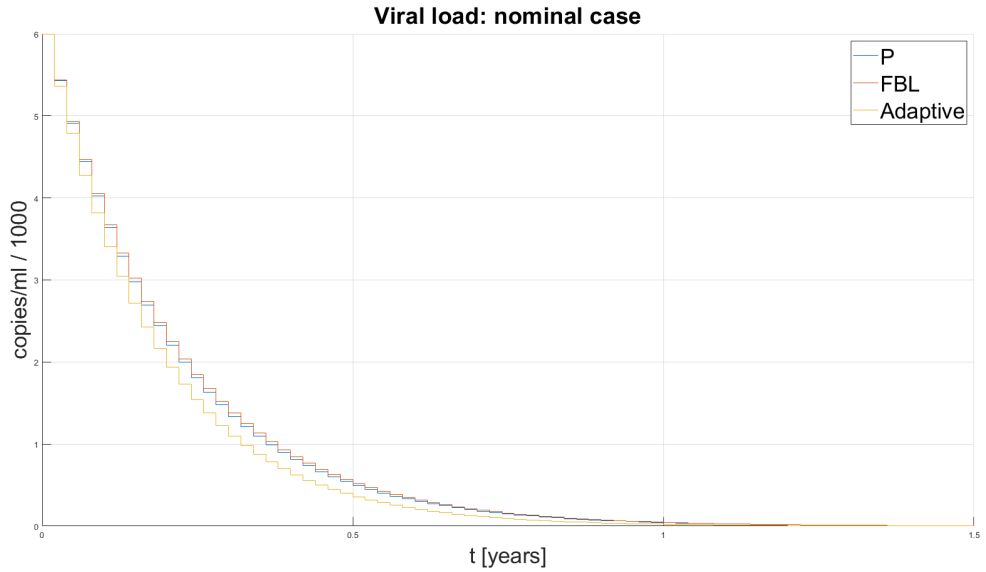

(a) *Viral load evolution.*

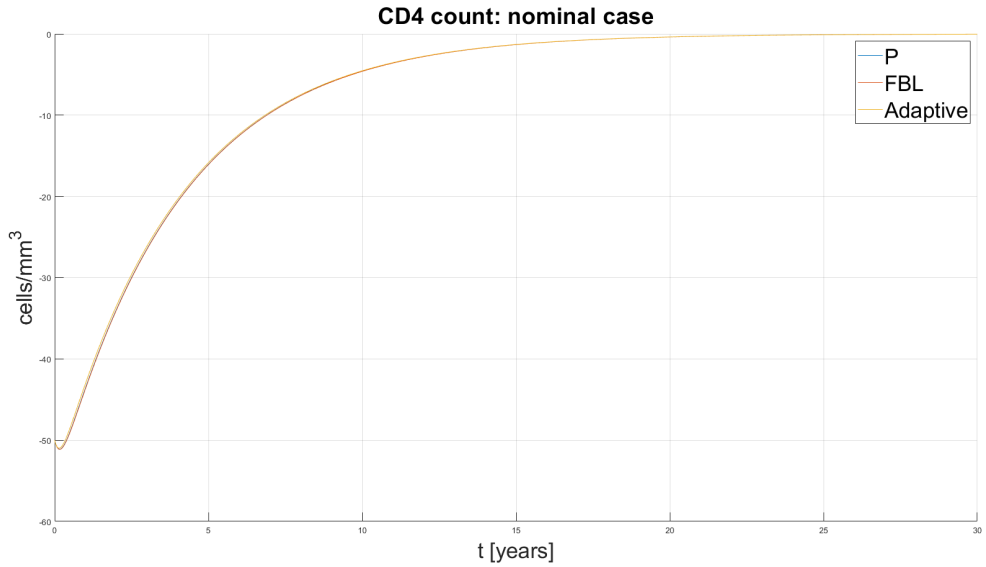

(b) *CD4 lymphocytes population evolution.*

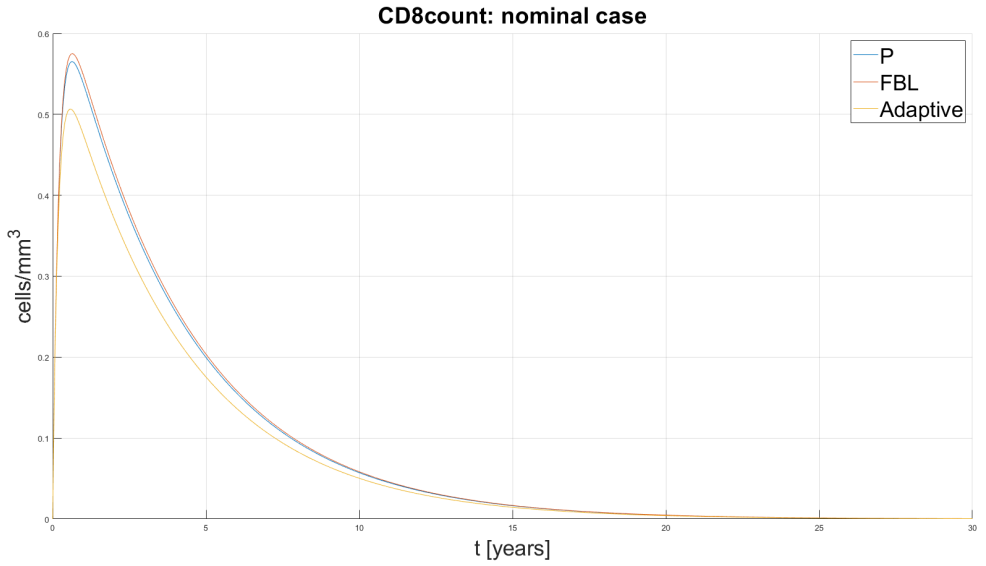

(c) *CD8 lymphocytes population evolution.*

Figure 3.11: Control comparison in ideal case: system's state evolution.

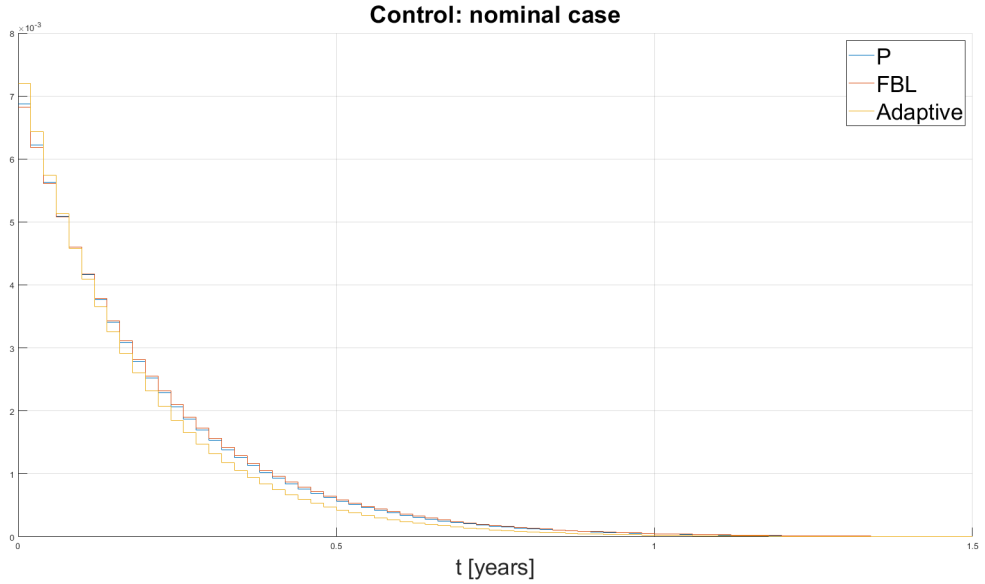

(a) *Control action.*

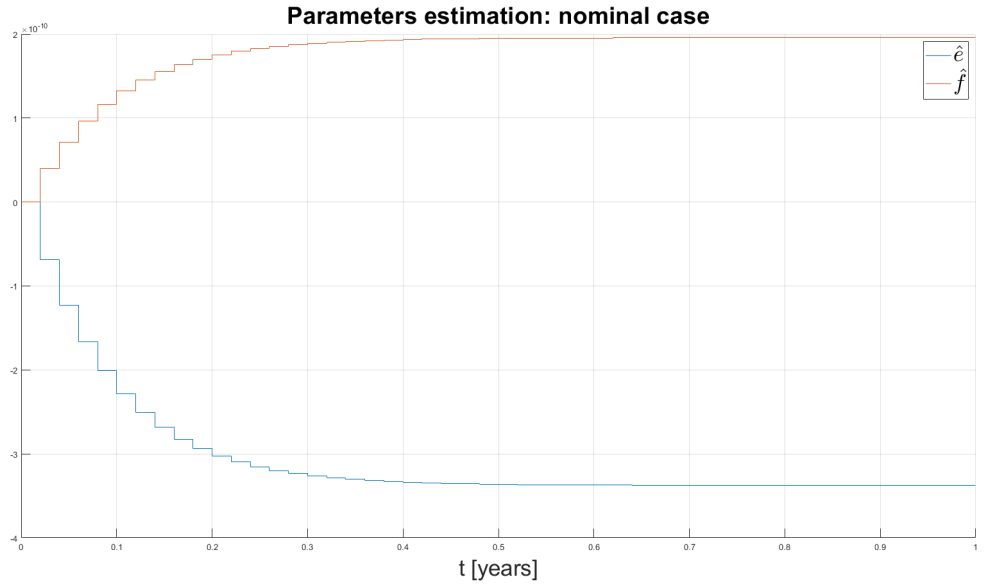

(b) *Parameter estimation.*

Figure 3.12: Control comparison in ideal case: control effort and parameter estimation.

Scheme	**Non-communicable time** [months]	**Steady state**	**Control peak** [$\cdot 10^{-3}$]
Proportional	13.39	virus-free	6.87
Feedback linearization	13.61	virus-free	6.83
Adaptive	11.62	virus-free	7.2

Table 3.3: Controls comparison with 5% parameter uncertainty.

3.4.2 5% parameter uncertainty

Consider now the case of a 5% paramer uncertainty on e and f. In particular, the worst case is considered, i.e., the maximum possible value of e and the minimum possible value of f:

$$e = 1.05\, e_{\text{nominal}} \qquad f = 0.95\, f_{\text{nominal}}$$

In Figures 3.13 and 3.14 the evolution of the control action, system's state and parameter estimation is presented. The performances of the three controls are summarized in Table (3.3).

Again, all the three control schemes are able to stabilize the system and nullify the viral load. However, only the adaptive control is able to achieve the non-communicability in under one year, while proportional and linearization both require one and a half month more.

Also, while the adaptive and proportional control peak are the same, the feedback linearization's one has increased, and it is much more similar to the other two.

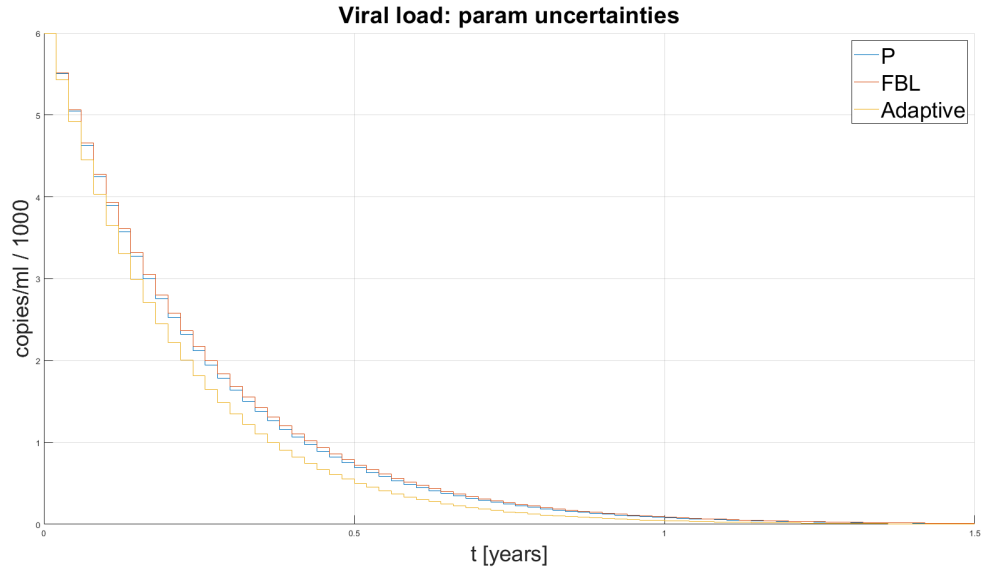

(a) *Viral load evolution.*

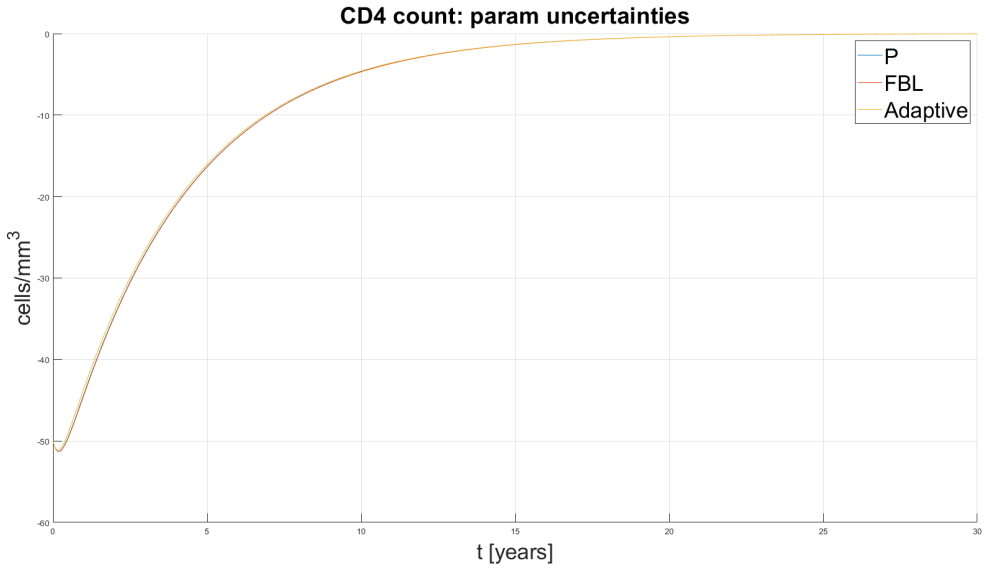

(b) *CD4 lymphocytes population evolution.*

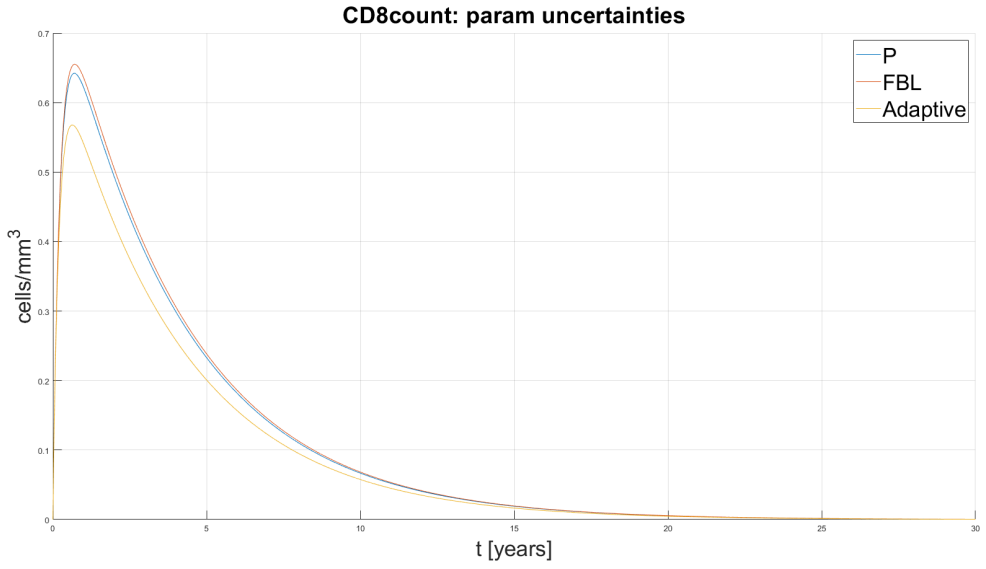

(c) *CD8 lymphocytes population evolution.*

Figure 3.13: Control comparison with 5% parameter uncertainty: state evolution.

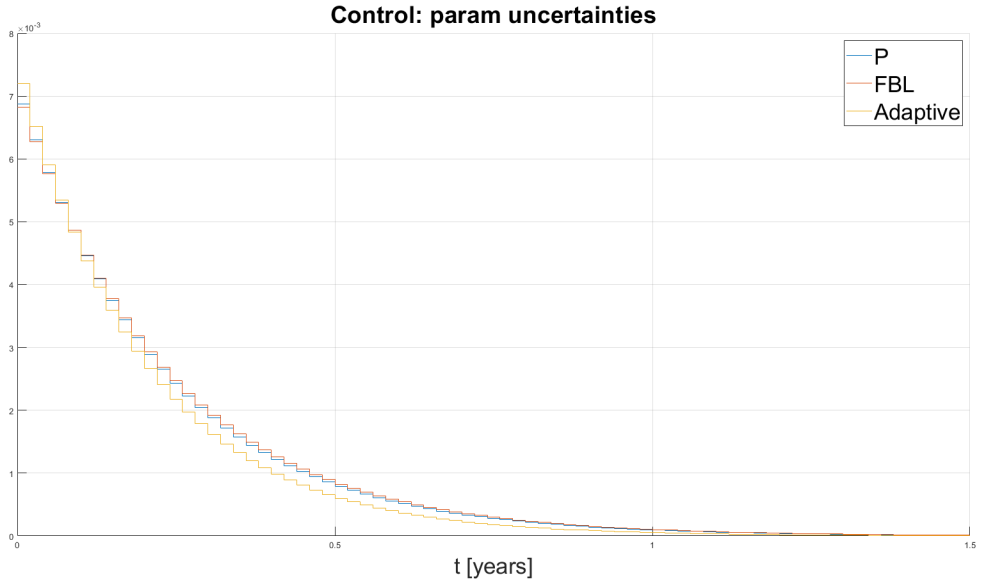

(a) *Control action.*

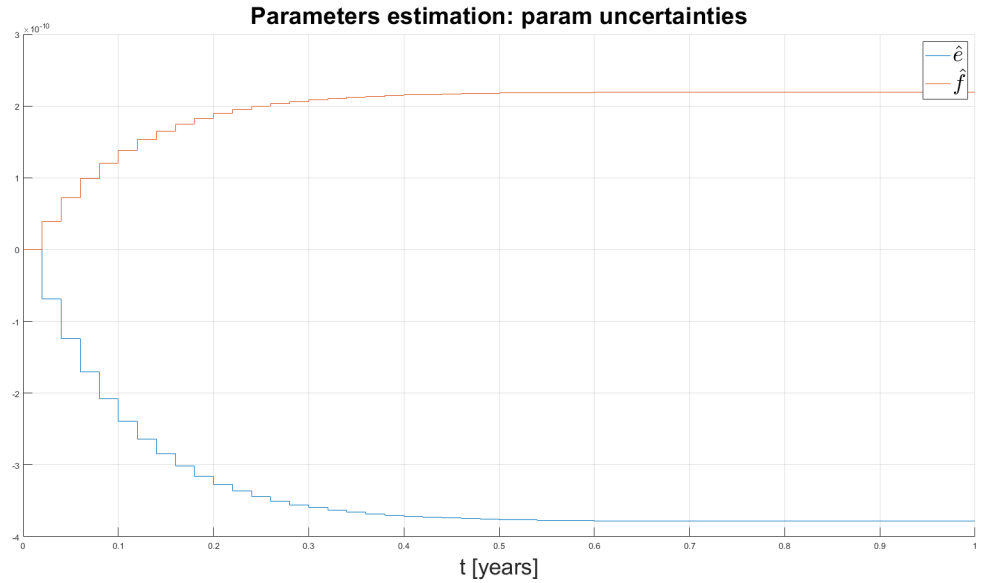

(b) *Parameter estimation.*

Figure 3.14: Control comparison with 5% parameter uncertainty: control effort and parameter estimation.

Scheme	**Non-communicable time** [months]	**Steady state**	**Control peak** $[\cdot 10^{-3}]$
Proportional	-	$[969, 554, 1595 \cdot 10^{-7}]$	6.87
Feedback linearization	-	$[991, 551, 412 \cdot 10^{-7}]$	6.83
Adaptive	81.79	virus-free	7.2

Table 3.4: Controls comparison with 35% parameter uncertainty.

3.4.3 35% parameter uncertainty

Consider now the case of a 35% paramer uncertainty on e and f; again, the worst case is considered, as the previous section:

$$e = 1.35\, e_{\text{nominal}} \qquad f = 0.95\, f_{\text{nominal}}$$

With this heavy uncertainty on the model knowledege, the adaptive control scheme is the only one able to nullify the viral load: however, this is done in 81.79 months ≈ 6.8 years: of course, this is not acceptable in a real application.

Proportional and feedback linearization approaches are not capable to take the viral load to zero; in particular, at the steady state there are 1595 and 412 copies/ml, respectively. The control action maximum values are pretty much the same as before.

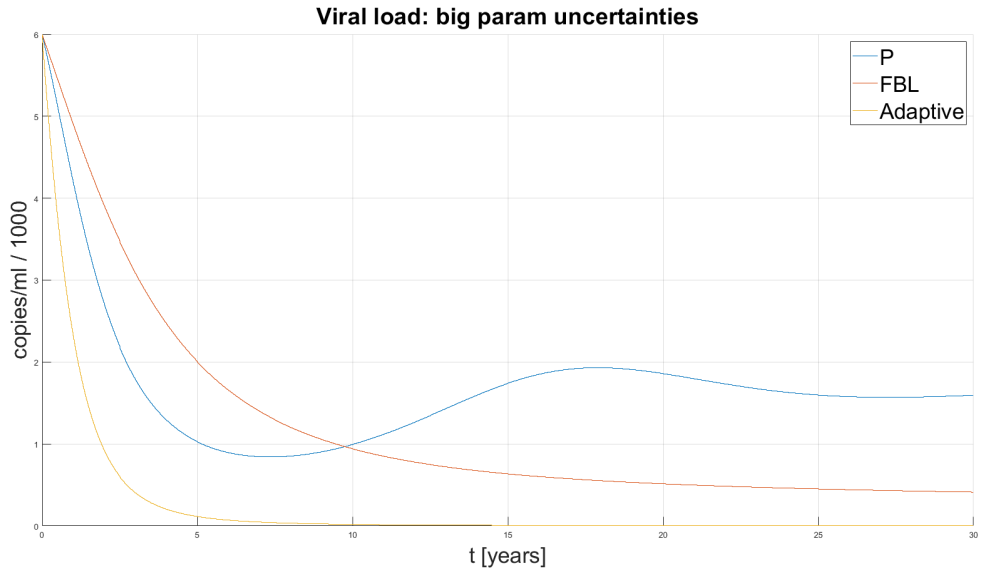

(a) *Viral load evolution.*

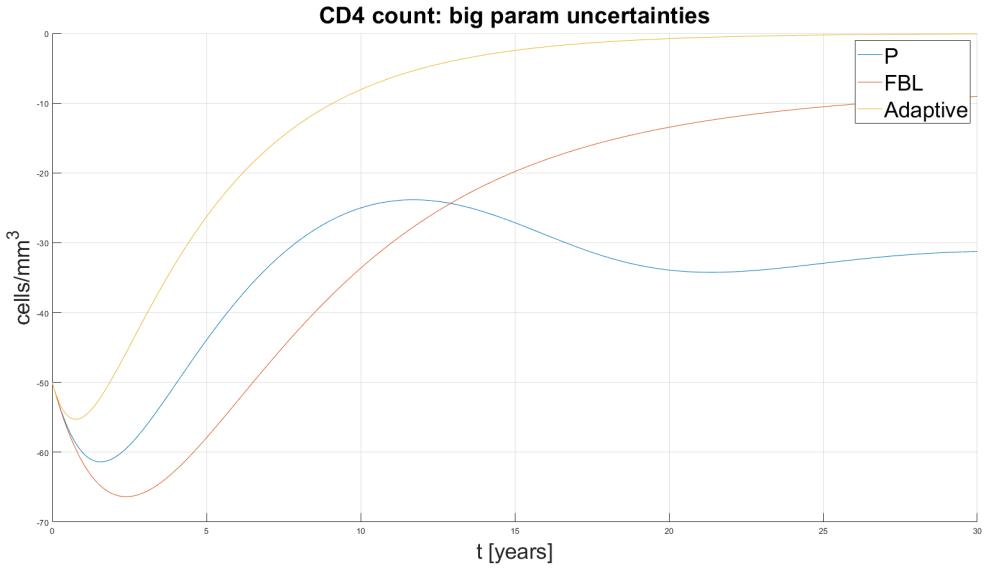

(b) *CD4 lymphocytes population evolution.*

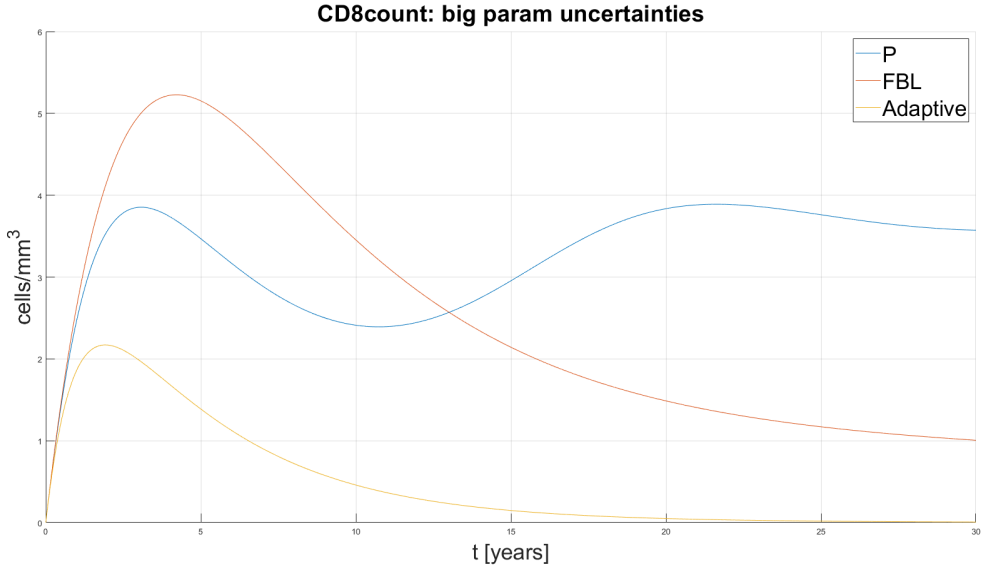

(c) *CD8 lymphocytes population evolution.*

Figure 3.15: Control comparison with 35% parameter uncertainty: state evolu-

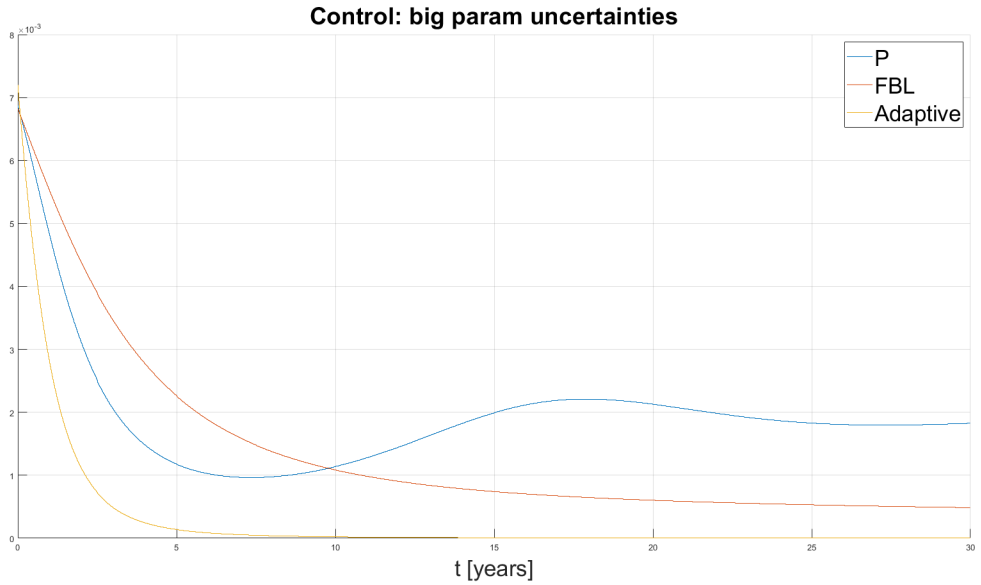

(a) *Control action.*

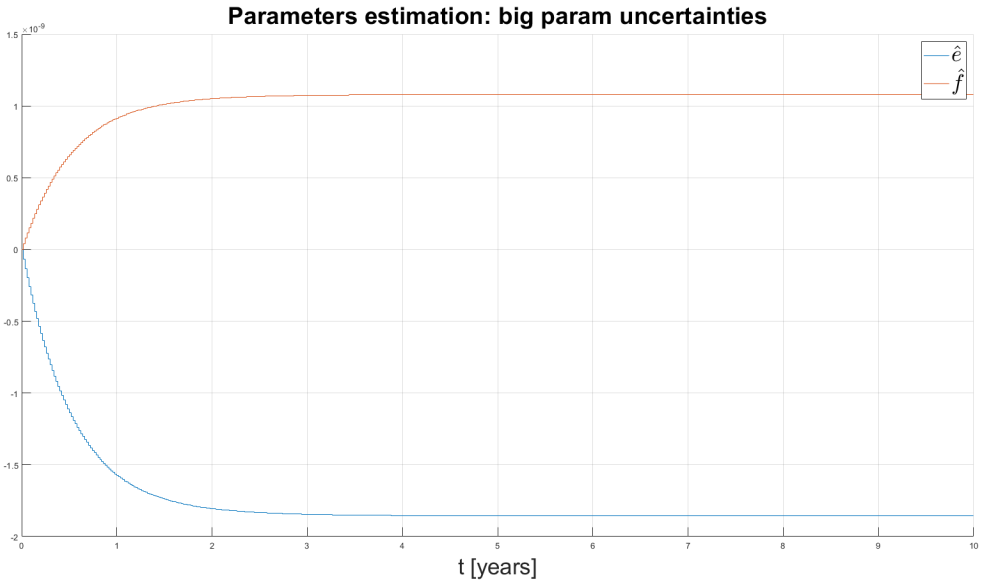

(b) *Parameter estimation.*

Figure 3.16: Control comparison with 35% parameter uncertainty: control effort and parameter estimation.

Scheme	**Non-communicable time** [months]	**Steady state**	**Control peak** $[\cdot 10^{-3}]$
Proportional	-	$[997, 550, 127 \cdot 10^{-7}]$	6.81
Feedback linearization	21.31	virus-free	6.8
Adaptive	-	$[997, 550, 455 \cdot 10^{-7}]$	7.13

Table 3.5: Controls comparison with measurement noise.

3.4.4 Measurement noise

Finally, consider the case of a measurement noise applied to the system's output, i.e., the viral load.

The idea is to provide a first approximation of the limitations of actual viral load measurements. In particular, tipically available tests are not capable to detect viral load under the 50 copies/ml threshold; moreover, they are always susceptible of errors. For these reasons, this has been modeled as a white noise in the range $[-75, -25]$ copies/ml added to the actual system's output; it is reported in Figures 3.17.

In this scenario, the feedback linearization scheme is the only one capable to nullify the viral load, requiring 21.31 months $\approx$ 1.78 years: again, this is not acceptable in a practical application.

The maximum control action value are practically the same as before.

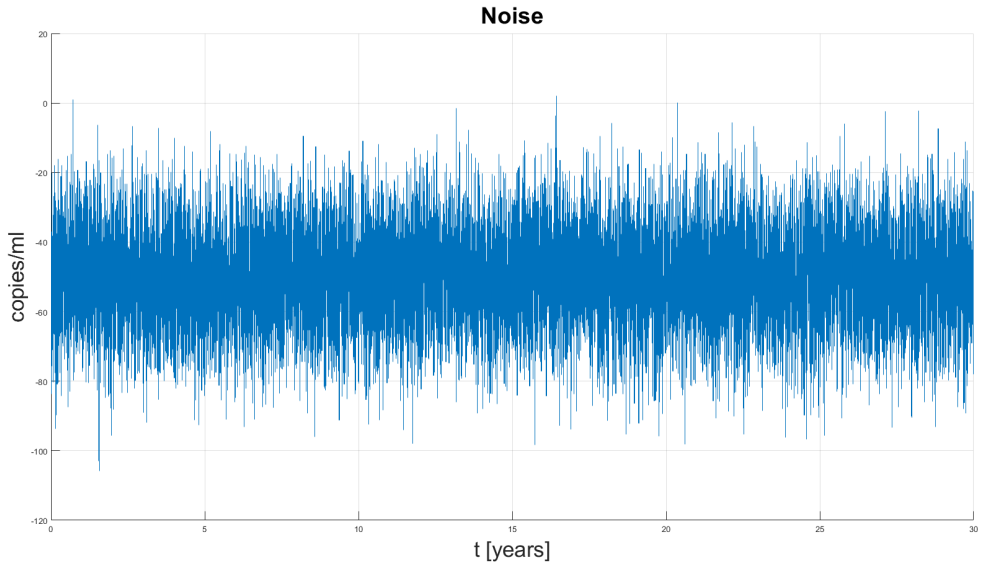

Figure 3.17: Noise applied to the system's output.

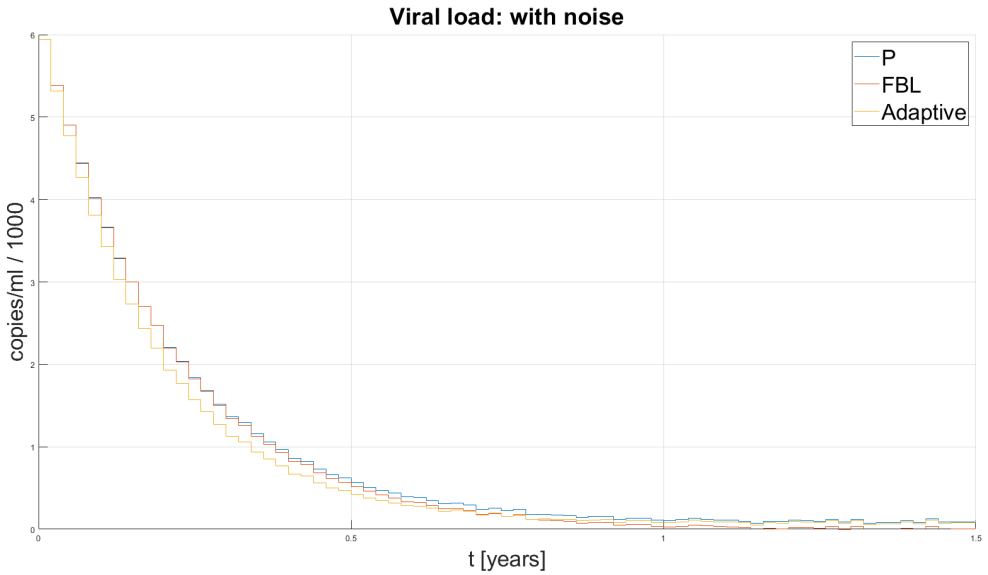

(a) *Viral load evolution.*

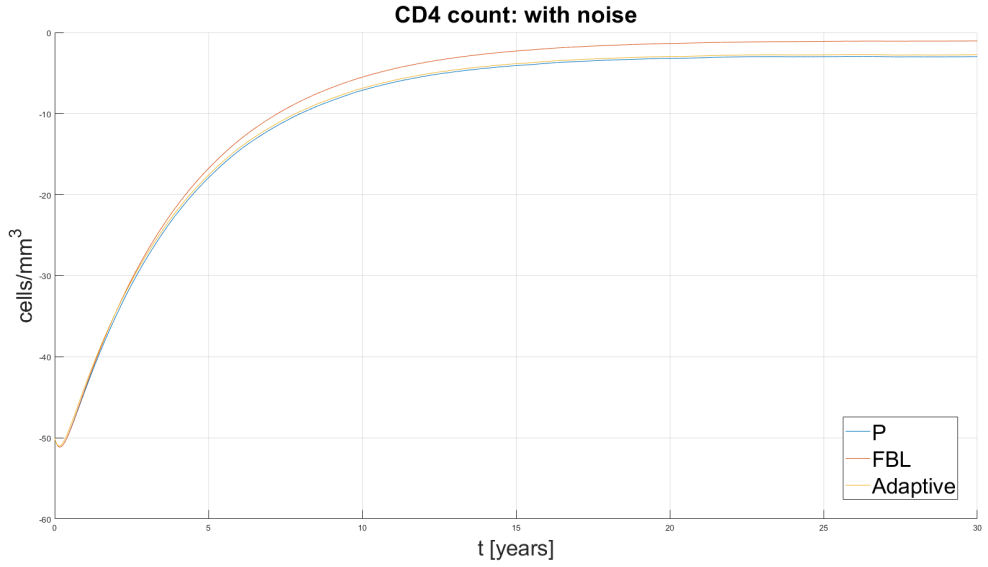

(b) *CD4 lymphocytes population evolution.*

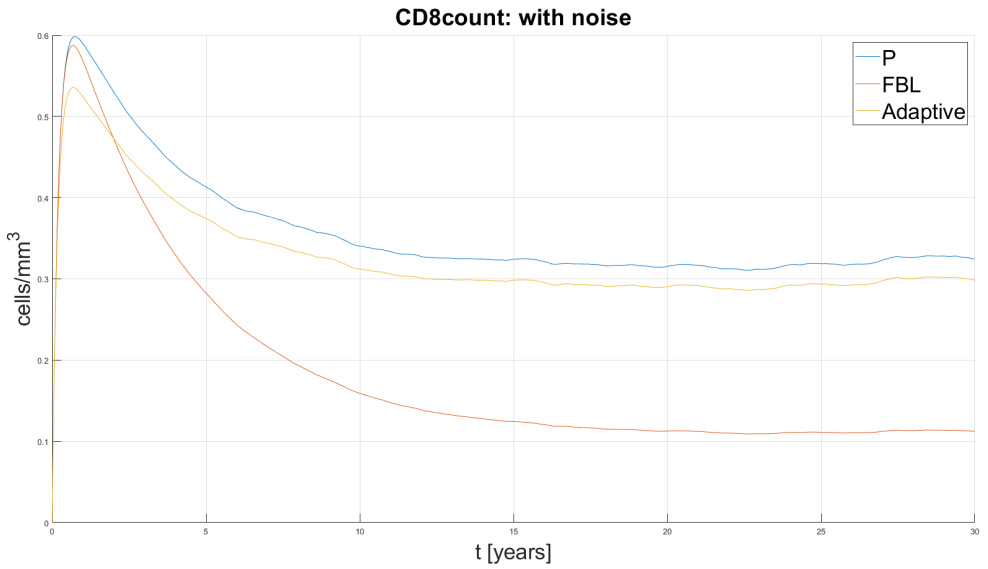

(c) *CD8 lymphocytes population evolution.*

Figure 3.18: Control comparison with measurement noise: state evolution.

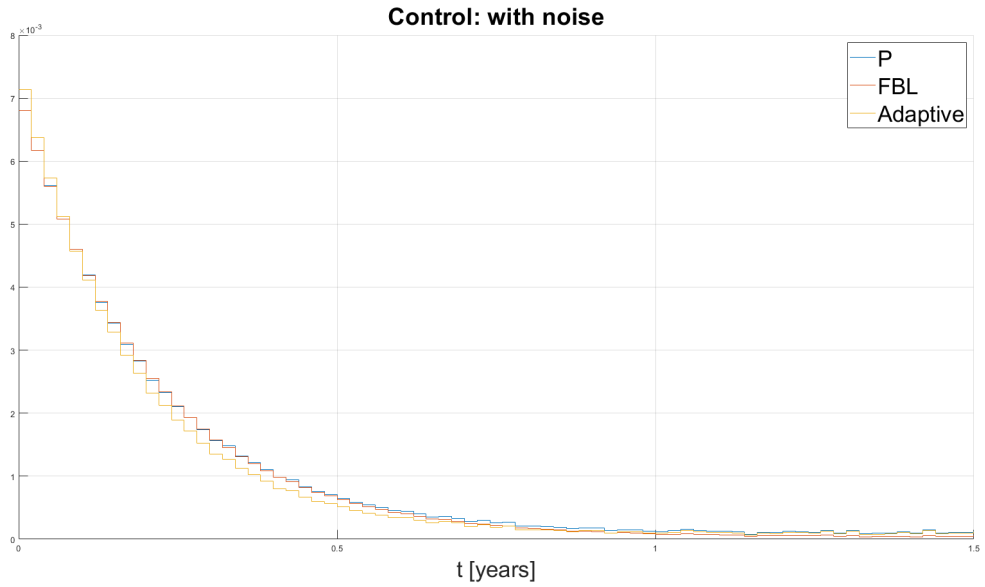

(a) *Control action.*

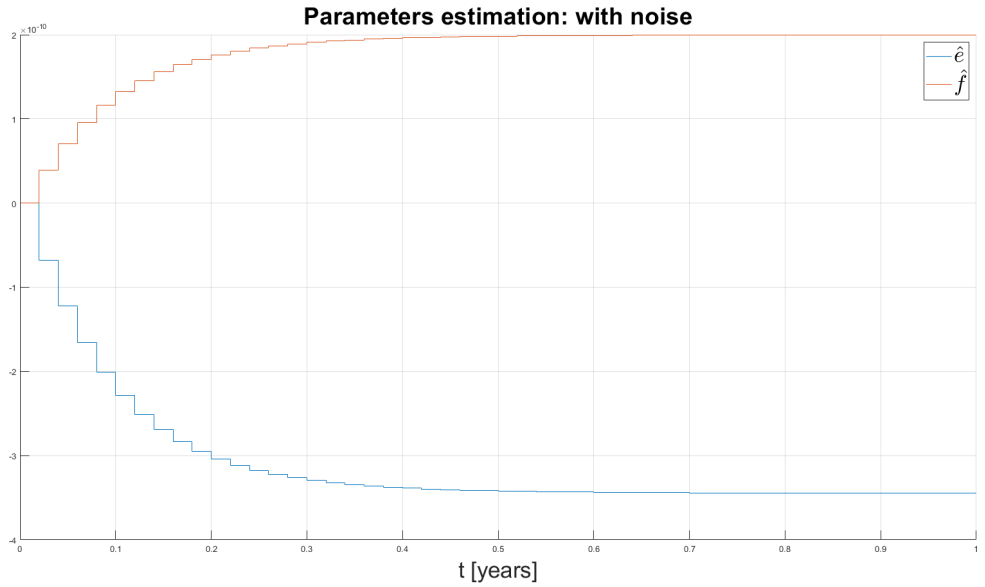

(b) *Parameter estimation.*

Figure 3.19: Control comparison with measurement noise: control effort and parameter estimation.

Chapter 4

Conclusions and further developments

In this paper, analysis and control of a biomedical model of HIV-1 infection in the human organism, as proposed in [5], has been carried out.

In particular, the model has been analyzed in depth: equilibria and their local and global stability has been discussed, a phase portrait has been sketched, and the presence of bifurcations has been studied.

Regarding the control, both linear and nonlinear controller schemes have been developed, tested and compared, with respect to realistic practical scenarios: the controllers have been discretized with a feasible (even if very expensive in practice) frequency, and parameter uncertainty has been considered too.

The controllers performances have been evaluated with respect to the speed of convergence of the viral load under the non-communicable threshold, and the maximum control effort: bigger control values means, indeed, heavier drug dosage and adversal effect for the patient, and so this is a crucial aspect to take into account.

With respect to these performance indeces, we can conclude that the best control scheme among the ones presented in this paper is the adaptive one.

In fact, in the practice the most likely scenario is the one with a relatively small parameter uncertainty on e and f: obtaining an accurate value of these two parameters represents today the biggest difficulty in studying and trying to model the dynamics of the HIV-1 infection.

A purely proportional controller could be a good and simple choice in the ideal scenario, but it is not reliable in presence of non-idealities.

Also, speaking about the scenario with measurement noise, it should be noted that the real cases are better than the one considered here. In fact, there exist new techniques able to detect the viral load down to 20 copies/ml; moreover, the tests are typically executed more than just one time, in order to obtain a more accurate result.

In any case, the results obtained in this paper show the importance of

working to develop good viral load measurement techniques, as well as the knowledge of the model parameters.

In the following, further developments are proposed for this research.

- Implementing the nonlinear controllers proposed here requires to measure the whole system's state. One possibility is to develop a state observer, in order to reduce the number and cost of exams the patient need to take.
- Another issue regards the controllers frequency. In this paper, a constant sample time of 1 week has been considered: even if this is feasible in practice, it would be extremely expensive. One possibility is to study the effects of a variable sample time, dense at the beginning of the treatment and more relaxed after.
- Exams tipically executed in labs are not able to detect the viral load under a threshold of 20 or 50 copies/ml. Since this issue has not been considered in this paper, when the viral load becomes undetectable another long term drug regimen should be considered.
- Finally, other control strategies should be considered too, like for example sliding mode control or model predictive control.

Bibliography

[1] Michael E. Brandt and Guanrong Chen. "Feedback control of biodynamical model of HIV-1". In: *IEEE Transactions on biomedical engineering* 48.7 (July 2001).

[2] B. S. Goh. "Global stability in many-species systems". In: *The American Naturalist* 111.977 (Jan. 1977), pp. 135–143.

[3] Hassan K. Khalil. *Nonlinear systems, 3rd edition.* Ed. by Inc. Prentice-Hall. 2002.

[4] Jean-Jacques E. Slotine and Weiping Li. *Applied nonlinear control.* Ed. by Inc. Prentice-Hall. 1991.

[5] Fernando Menezes Campello de Souza and al. "Modeling the dynamics of HIV-1 and CD4 and CD8 Lymphocytes". In: *IEEE Engineering in medicine and biology* (Jan. 1999).

[6] UNAIDS, ed. *Undetectable = untransmittable: public health and HIV viral load suppression.* URL: `https://www.unaids.org/sites/default/files/media_asset/undetectable-untransmittable_en.pdf`.